TAMPEREEN TEKNILLINEN YLIOPISTO
TAMPERE UNIVERSITY OF TECHNOLOGY

SUBARNA BHATTARAI

CONDUCTING POLYMERS IN AUGMENTING THE PROPERTIES OF BIOPOTENTIAL ELECTRODES

Master of Science Thesis

Examiners: Professor Jari Hyttinen and Minna Kellomäki

Examiners and topic approved by the Dean of the Faculty of Computing and Electrical Engineering on 26th April 2017.

ABSTRACT

SUBARNA BHATTARAI: Conducting Polymers in Augmenting the Properties of Biopotential Electrodes
Tampere University of Technology
Master of Science Thesis, 74 pages, 1 Appendix page
March 2017
Master's Degree Programme in Electrical Engineering, MSc (Tech)
Major: Medical Instrumentation
Examiner: Professor Jari Hyttinen and Minna Kellomäki

Keywords: Polypyrrole, biopotential electrodes, electrode-electrolyte interface, impedance magnitude and phase, morphology

Conducting polymers, especially Polypyrrole (PPy), have been extensively used for the modification of the electrode surface by electrochemical deposition. The combination of carbon nanotubes (CNTs) and PPy has also been successfully electrodeposited on the electrode surface to lower the impedance. The morphology of such coated electrode were also found to be rougher than PPy or CNT alone which could indicate greater electroactive area of the coated film.

The thesis is based on electrodeposition of two types of biopotential electrodes: a) Microelectrode arrays (MEAs) and b) Macroelectrodes. The electrodeposition process was evaluated by chronopotentiometric measurement by measuring the charge and current density.

The PPy and PPy/CNT solutions were successfully electrodeposited onto the Platinum(Pt) macroelectrode surface. PPy/CNT decreased the macroelectrode impedance. Optical Profilometer analysis showed that PPy-CNT 0.25 sample (made from 0.25mg/ml of CNT) produced the roughest surface and PPy-Control sample produced the smoothest surface. Atomic Force Microscopy(AFM) analysis showed that the PPy-CNT 0.5 sample (made from 0.5mg/ml of CNT) was more rougher than the PPy surface. Micrograph analysis showed thick coating with PPy-CNT 0.25 and PPy-CNT 0.5 samples than PPy-Control and PPy-CNT 0.1 (made from 0.1mg/ml of CNT) samples.

A wide range of electrical properties were also observed in different frequencies. PPy-CNT 0.5 was highly resistive at 1kHz with phase angle of 29° and most capacitive at 1.0Hz with phase angle of -68°compared to coated electrodes. PPy-CNT 0.25 showed maximum impedance magnitude at 1.0Hz and PPy-CNT 0.5 showed least magnitude at 1KHz. Bare Pt was highly capacitive at 1Hz with the phase angle of -78°. PPy-CNT 0.5 was highly capacitive at lower frequencies (<100Hz) than any other coated electrodes while PPy-CNT 0.25 was most resistive.

Plasma treatment reduced the MEAs impedance. However, the MEA was not coated with PPy solution. Variations in charge and current densities was observed with MEAs electrodeposition. These types of electrodeposition analysis could be useful in future research to characterize the impedance of the coated film to improve the performance of biopotential electrodes.

PREFACE

I would like to thank my professors Jari Hyttinen and Minna Kellomäki for their support and guidance throughout my thesis work.

I would like to thank my supervisor, MSc.Virpi Alarautalahti, for her immense support and help. I would like to thank Sister Richards for her inspiration, love and support that she has given me to write this project.

I would like to thank my family and friends for trusting me.

Tampere, 21.3.2017

Subarna Bhattarai

CONTENTS

LIST OF FIGURES

LIST OF TABLES

LIST OF SYMBOLS AND ABBREVIATIONS

AFM	Atomic Force Microscopy
CE	counter electrode
CNTs	carbon nanotubes
COOH	Carboxylic acid
SWCNTs	Single-walled CNTs
DBS	Dodecyl-benzene sulphonate
DI	deionized
E	Electrode
eV	electron Volt
EDOT	3,4-ethylenedioxythiophene
EIS	Electrochemical Impedance Spectroscopy
h	hour
MeOH	Poly(hydroxymethyl)
MWCNTs	Multi-walled CNTs
Pani	Polyaniline
PBS	Phosphate buffer solution
PEDOT	poly(3,4-ethylenedioxythiophene)
PPy	Polypyrrole
PSS	Poly(styrenesulfonate)
PTh	Polythiphene
Py	Pyrrole
WE	Working electrode

1 INTRODUCTION

Biopotential electrodes are generally used for recording and stimulating the bioelectric signals. The bioelectric potentials in the electrolytic media are transduced by the electrodes into electronic signals by means of (Frölich et al. 1996; Weiland & Anderson 2000):

a) Capacitive coupling (without net charge transfer) which happens during recording and b) charges transfer reactions in which the ions in the physiologic environment exchange electrons on electrodes through redox reactions. This process happens mainly during stimulation. These reactions could be reversible or irreversible generating gases at the electrode site and leading to tissue damage and electrode corrosion due to its oxidation.

It is not so clear that the recording would be capacitive and stimulus require charge transfer, so it is possible to have a capacitive electrode for both recording and stimulation. Similarly we can have good Ag-AgCl electrodes with lower capacitance that can be used for recording. Thus this transduction phenomena depends on the type of electrodes used.

One important goal of electrode fabrication is the low impedance. With the small microelectrode size, the recording and stimulation can be confined to a single cell or neuron, thus preventing the interference with the neighboring cells. Hence, high-density microelectrodes with a large number of electrode sites could be useful. However, this decreases the geometric area of the electrodes and results in higher electrode impedance thus high electronic noise during recording. Also, the safe injection charge through an electrode to stimulate the cells is reduced. These factors presents a major drawback when using a small surface area electrode. One way to decrease the electrode impedance is to coat the electrode with electrically conducting polymers, whose nodular surface topography increases the active surface area of the electrode. The two most important criteria/limitations for electrodes selection are: a) surface area of the electrode and b) charge transfer capacity between electrode and cell. (Heim et al. 2012)

Various biopotential electrodes have been coated with the conducting polymers to reduce the electrode impedance and to improve the electrical properties of the electrode. Electrochemical Impedance Spectroscopy has been extensively used to measure the electrical properties of the coated surface and to predict and build several electrical models of the electrode-electrolyte interface (Xiao et al. 2004; Abidian & Martin 2007; Harris et al. 2013).

Conducting polymers (CPs) are a special class of polymeric materials with electronic and ionic conductivity. Their porous structures and electric conductivity (Schultze & Karabulut 2005) allow them to be used in dry as well as in wet state (Xu et al. 2005).

The conducting and semi conducting properties of CPs have made them an important class of material for a wide variety of applications (Ravichandran et al. 2010). The scope of CPs in biomedical engineering application includes the development of artificial muscle (Otero & Sansinena 1998), controlled drug release (Abidian et al. 2006), neural recording (Abidian et al. 2009) and the stimulation of nerve regeneration (Schmidt et al. 1997). CPs can be easily fabricated by electrochemical method where they can be deposited on the surface of a given substrate. This allows producing a polymer surface whose thickness and formation rate can be controlled (Vidal et al. 2003).

CPs can be physically or chemically modified. Chemical modification has been studied by using biomolecules as dopants (Cui et al. 2003) or by immobilizing bioactive molecules on the surface of the material (Zhong et al. 2001). Physical modification has been done by increasing the surface roughness of the material by various methods such as creating microporous films, fabricating nanoparticles and nanopeptides, growing CPs within hydrogel and blending CPs with biomolecules to produce 'fuzzy' structures (Ravichandran et al. 2010). The increased surface roughness due to CPs coating increases the surface area of the electrodes and hence lowers the electrode impedance. Among CPs, Polypyrrole (PPy) is one of the most studied electroactive conducting polymers for coating the electrode surface to lower the impedance. It can be doped with various reagents to change its physical, chemical and electrical properties.

Carbon nanotubes (CNTs) are built from carbon units, which have seamless structure with hexagonal honeycomb lattices. They have closed topology and tubular structure, and they are several nanometers in diameter (Caglar 2017). They are widely used in electroanalytical applications because of their ability to promote electron transfer and provide stable polymer film coatings. It is one of the most important materials used in nanotechnology. The PPy/CNT has been successfully electrodeposited and it has shown better electrical results than PPy or CNT alone (Shaffer et al. 1998; Han et al. 2005; Almohsin et al. 2012). The combination of PPy and CNT has been used in several electrochemical applications to characterize the behaviour of the coated surface. Such applications include electrochemical supercapacitors (Li & Zhitomirsky 2013) and CNT/PPy electrodeposition on glassy carbon electrode (GCE) for neurotransmitter detector sensor (Agui et al. 2008).

The purpose of this thesis was to coat platinum electrodes having two dimensions, microscopic electrodes (microelectrode arrays, MEAs) and macroscopic electrodes. The MEAs was coated with PPy while macroelectrodes was coated both with PPy and PPy/CNT. For fabrication, we used the electrochemical method. The coated films were then characterized by measuring the impedance and surface imaging.

2 THEORETICAL BACKGROUND

2.1 Conducting polymers

The unique feature of the conducting polymer is the conjugated molecular structure of the polymer main chain where the π-electrons delocalize over the whole polymer chain. Conjugated polymers becomes conducting after the doping process. Among the conjugated polymers, polyacteylene has the simplest chain structure composed of an alternate single bond and double bond carbon chain. According to the locations of the hydrogen atoms on the double bond carbons, there are two kinds of structures: *trans*-polyacetylene and *cis*-polyacetylene as shown in Figure 2 below. In *trans*-polyacetylene structure, the two hydrogen atoms are located on the opposite side of the double bond carbon whereas in *cis*-polyacetylene structure, the two hydrogen atoms are located on the same side of the double bond. *trans*-polyacetylene is a degenerate conjugate polymer which possesses an equivalent structure after exchanging it's single and double bonds. *cis*-polyacetylene is nondegenerate conjugated polymer which have non-equivalent structures after exchanging it's single and double bonds. The structures of various conjugated polymers is shown in Figure 1 below. (Li 2015)

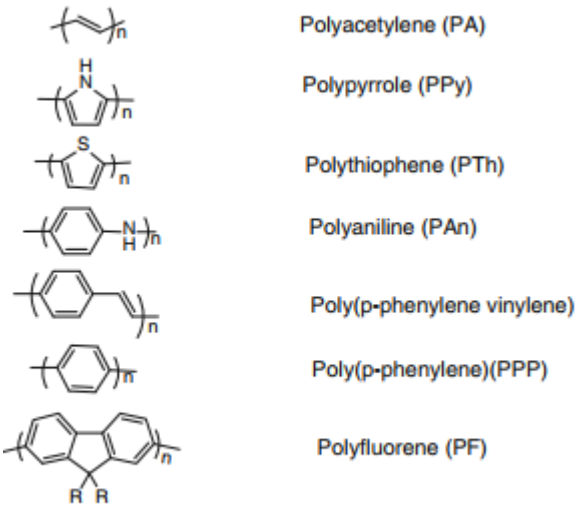

Figure 1: Main chain structures of several representative conjugated polymers (Li 2015).

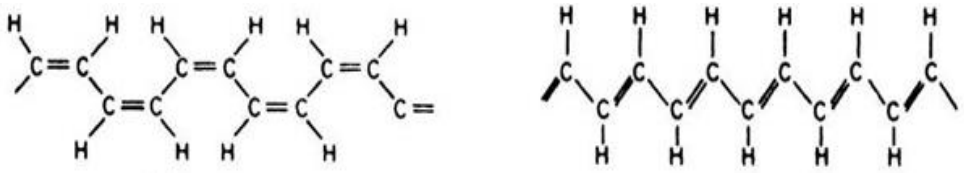

a) b)

Figure 2: Isomers of polyacteylene a) cis-polyacteylene and b) trans-polyacetylene (Goh et al. 2009).

Conjugated polymers possess delocalized π-electron structure, which includes the band structure of π-valence band and π*-conducting band. In the basic state of intrinsic conjugated polymers, all the valence bands are filled by electrons and all the conduction bands are empty. The difference between the top of the valence band (the highest occupied molecular orbital) and the bottom of the conduction band (the lowest unoccupied molecular orbital) is called the bandgap (*Eg*). The *Eg* values of most conjugated polymers are in the range 1.5-3.0 electronVolt (eV). Therefore, the intrinsic conjugated polymers are organic semiconductors. (Li 2015)

2.1.1 Doping structures of conducting polymers

The unique feature of conducting polymers is the p-doped and n-doped states of the conjugated polymer main chain. In the p-doped state, the main chain of the conducting polymer is oxidized with counterion to maintain the electron neutrality of the whole molecule. There are holes in the main chains (lost electrons) which makes the conducting polymer p-type conducting. In the n-doped state, the main chain of the conducting polymer is reduced with counterion to maintain the electron neutrality of the whole molecule. There are electrons in the main chains which makes the conducting polymer n-type conducting. (Li 2015)

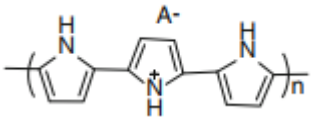

Figure 3: p-Doped structure of conducting PPy (Li 2015).

Figure 3 shows the p-doped structure of the conducting PPy. The positive charge is delocalized on the PPy main chain. A^- represents counteranions such as nitrate (NO_3^-), chlorate (ClO_4^-), chloride (Cl^-).

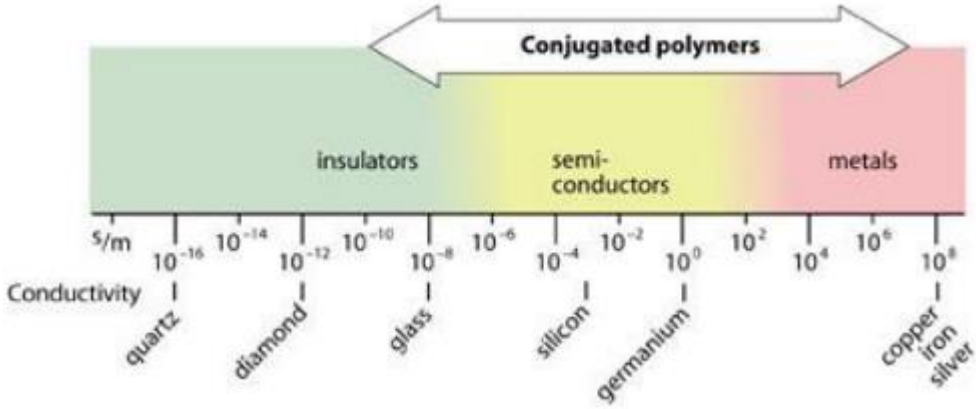

Figure 4: Conductivities of insulators, semi-conductors, metals and conjugated polymers (The Nobel Prize in Chemistry 2000).

The number of counteranions per monomer unit of the conducting polymer (or the concentration of the charge carrier in the conjugated main chain of the conducting polymer) is called the doping degree of the conducting polymer. The maximum doping degree is related the main polymer chain structure. For example, the doping degree for polyacetylene is usually 0.1-0.2, 0.25-.0.35 for polypyrrole, 0.4-0.5 for polyaniline, 0.3-0.4 for polythiophene. For the p-doped polypyrrole, the doping degree of 0.25-0.35 implies that the conjugated chain including 3-4 pyrrole units can be doped with 1 counterion (or there is a hole within the polypyrrole main chain containing 3-4 pyrrole units), as shown in Figure 3. The doping degree is much higher in conducting polymers where the charge carrier concentration reaches 10^{21} /cm^3. This value is several orders higher than that of inorganic semiconductors as shown in Figure 4. In addition, the doping in conducting polymers also results in morphology changes and volume expansion because of the counteranion doping. (Li 2015)

2.1.2 Charge carriers in conducting polymers

For *trans*-polyacetylene with the degenerate basic state, the charge carriers are polarons and solitons. For the basic state nondegenerate cis-polyacetylene, PPy, PTh, Pani. the charge carriers are polarons and bipolarons. The soliton is an unpaired π-electron resembling the charge on free radicals. It can be delocalized on a conjugated polymer chain. The neutral soliton can be oxidized to lose an electron and form a positive soliton, or it can be reduced to gain an electron to become negative soliton. The soliton possesses a spin of 1/2 whereas there is no spins for positve and negative solitons. Polarons are the major charge carriers in conducting polymers including basic state degenerate *trans*-polyacetylene and the basic state non degenerate conjugated polymers. P^+ denotes positive polaron which is formed after oxidation of the conjugated polymer main while and P^- denotes negative polaron which is formed after the reduction of the conjugated polymer main chain. P^+ and P^- possess spin of 1/2. (Li 2015)

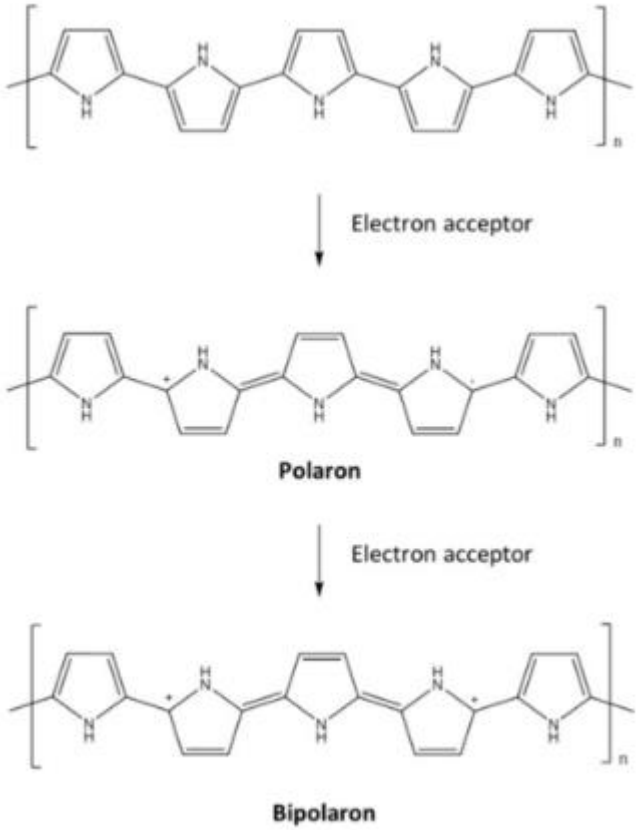

Figure 5: Polaron and bipolaron formation upon oxidation (p-doping) of polypyrrole (Jangid et al 2014).

The bipolaron is the charge carrier that possesses double charges by coupling of two P^+ or two P^- on a conjugated polymer main chain. It has no spin and can be formed when the concentration of polarons are high in the conjugated polymer main chains. The positive bipolaron and negative bipolaron correspond to the hole pair or the electron pair. Figure 5 shows the polaron and bipolaron structure of polypyrrole upon oxidation. (Li 2015)

2.1.3 Doping characteristics

Doping of conducting polymers can be realized chemically or electrochemically by oxidation or reduction of the conjugated polymers. (Li 2015)

2.1.3.1 Chemical doping

The chemical doping includes p-type doping and n-type doping. p-Doping is also called oxidation doping, which refers to the oxidation process of the conjugated polymer main chain to form polarons. The oxidants like Iodine (I_2), Bromine (Br_2), Arsenic pentafluoride (AsF_5), etc. can be used as p-dopants. After p-doping, the conjugated polymer is oxidized and loses electron to form p-doped conjugated polymer chain, and

the dopant gains an electron to become the counteranion. The p-doping process can be realized from the following reaction:

$$CP + (3/2)I_2 \rightarrow CP^+(I_3^-) \quad (1)$$

where CP denotes conducting polymers.

n-Doping is also called reduction doping, which refers to the reduction process of the conjugated polymer main chain to form negative charge carriers. The reductants like alkali metal vapor, sodium naphthalenide (Na^+ $(C_{10}H_8)^-$), etc. can be used as n-dopants. After n-doping, the conjugated polymer is reduced and gains electron to form n-doped conjugated polymer chain, and the dopant losses an electron to become the countercation. The n-doping process can be realized from the following reaction:

$$CP + Na^+(C_{10}H_8)^- \rightarrow CP^-(Na^+) + C_{10}H_8 \quad (2)$$

where CP is the conducting polymer.

2.1.3.2 Electrochemical doping

Electrochemical doping is realized by electrochemical oxidation of reduction of the conjugated polymers on an electrode. For electrochemical p-doping, the conjugated polymer main chain is oxidized to lose an electron (gain a hole) where the doping of counteranions is accompanied from electrolyte solution :

$$CP - e^- + A^- \rightleftharpoons CP^+(A^-) \quad (3)$$

where A^- denotes the solution anion, $CP^+(A^-)$ represents the main chain oxidized conducting polymer and counteranion doped. (Li 2015)

For electrochemical n-doping, the conjugated polymer main chain is reduced to gain an electron where the doping of countercations is accompanied from electrolyte solution:

$$CP + e^- + M^+ \rightleftharpoons CP^-(M^+) \quad (4)$$

where M^+ denoted solution cation, $CP^-(M^+)$ represents the main chain reduced conducting polymer polymer and countercation doped. (Li 2015)

The electrochemical doping is simple and reproducible, and it can be carried out amperometrically or potentiostatically or with a cyclic scan of a potential (voltammetric). (George et al. 2006) It is usually performed in an electrochemical cell.

The electrochemicall cell can be of three types used to fabricate the conducting polymers: (Yang & Martin2004).

a) current-controlled (galvanostatic) method: A current source is attached between working and counter electrodes and a user-defined current is passed.

b) voltage-controlled (potentiostatic) method: A current is pushed between working electrode and counter electrode as required to control the working electrode potential with respect to a reference electrode.

c) V_{WE-CE} control (voltammetric): A voltage source is applied between the working and counter electrodes. The potential of these electrodes with respect to reference electrode are not controlled. Here only the net potential between working and reference electrodes are controlled.

The electrodeposition process is very fast, and takes usually a few seconds. The film thickness can be easily calculated with the measurement of total charge in the formation of CPs. In the same way, the final potential and the anion (or anions) of the supporting electrolyte regulates the level of doping as well as the oxidation state and conductivity of polymer. The final polymer can reach conductivities upto $1.0\text{-}10^5$ S/cm. (George et al. 2006)

2.1.4 Application of CPs

Conducting polymers (CPs) are discovered over 30 years ago with a growing interest on their electronic conducting properties and unique biophysical properties. Some of the applications of the CPs are:

a) Chemical sensors: Conducting polymers such as PPy, Pani, PTh, and their derivatives have been used as the active layers of the gas sensors (McQuade et al. 2000).

b) Drug delivery: The biocompatibility of CPs opens up the possibility for them to be used as in vivo biosensors applications for continuous monitoring of drugs or metabolites in biological fluids (Harwood & Pouton 1996).

c) Bioactuators: Bioactuators are the device which are used to create mechanical force, which in turn can be used to create artificial muscles. The process of change in the volume of CP scaffold upon electrical stimulation has been amployed in the development of bioactuators (Ravichandran et al. 2010).

d) Tissue engineering applications: The desired properties of CPs for tissue engineering applications are conductivity, reversible oxidation, redox stability, biocompatibility, hydrophobicity, three-dimensional geometry and surface topography. They are widely used in tissue engineering applications because of their ability to subject cells to an electrical stimulation (Ravichandran et al. 2010).

e) Biosensors: CPs acts as an excellent materials for the immobilization of biomolecules and fast electron transfer for the development of efficient biosensors. They are used to enhance speed, sensitivity and versatility of biosensors in diagnostic medicine to measure vital analytes in the human body and thus are widely used in medical diagnostic reagents (Heller 1990).

They have also attracted much interest as a suitable matrix for the entrapment of enzymes. The ideas of incorporating of enzymes into electro-depositable conducting polymeric films permit the localization of biologically active molecules on electrodes of any size or geometry, mostly for the fabrication of multi-analyte micro-amperometric biosensors. (Unwin & Bard 1992)

They are also known to be compatible with biological molecules in neutral aqueous solutions. They can be reversibly doped and undoped electrochemically along with significant changes in conductivity and spectroscopic properties of the film that can be used as a signal for the biochemical reaction. The electronic conductivity of CPs changes in response to change in pH and redox potential of their environment. (Paul et al.1985)

They have the ability to transfer electric charge produced by biochemical reaction to electronic circuit. It can be deposited over a desired area of electrodes. This property of CPs together with the possibility to entrap enzymes during EP has been exploited for the development of amperometric biosensors. (Foulds & Lowe 1986)

Other applications include corrosion protection layer, solar cells, Field-Effect Transistor (FET) sensors and chemiresistors (Gerard et al. 2002).

2.1.5 Polypyrrole

Polypyrrole (PPy) is an electrically conducting polymer that can be polymerized electrochemically and deposited onto the electrodes. PPy is one of the most widely studied electroactive conducting polymer because of its solubility in aqueous solution and low oxidation potential of the monomer, ease of use, controllable surface properties and compatibility with the mammalian cells. (Harris et al. 2013) It can be doped with various counterions ions to change its physical, chemical and electrical properties (George et al. 2005). The ability to control PPy surface properties such as charge density and wettability initiate the potential for modifying neural interactions with the polymer (Cui et al.2001). It enables flexibility in the design of three-dimensional polymer implants because of ease of fabrication and the ability to control its growth rate (Lavan et al. 2003). PPy is a relatively soft material when coated on the surface of the electrodes which promotes cell attachment onto the surface (Heim et al. 2012).

2.2 Carbon nanotubes (CNTs)

CNTs are one of the most commonly used building blocks of nanotechnology. They are used in various commercial products like rechargeable batteries, automotive parts and sporting goods. Advancement in CNT synthesis, purification and modification have enabled them to be use in thin-film electronics and large-area coatings. Although they do not have compelling mechanical strength or electrical or thermal conductivities, CNTs have shown promising performance for application including supercapacitors, actuators and lightweight electromagnetics shields (Volder et al. 2013). The properties of CNTs, such as high electronic conductivity and high mechanical resistance have driven extensive research in recent years mostly in the field of electroanalytical chemistry. The ability of CNT's to promote electron transfer in electrochemical reactions is the main reason for its successful use in electroanalytical applications. It has been widely used in design and testing of various biological and electrochemical sensors (Agui et al. 2008; Vairavapandian et al. 2008). It has single-walled and multi-walled structures as shown in Figure 1.

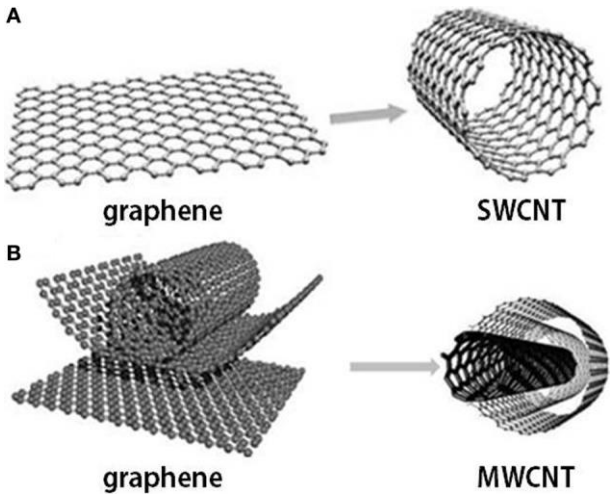

Figure 6: A) Single-wall CNT and B) Multi-wall CNT (Vidu et al. 2014).

Single-walled CNTs (SWCNTs) are made of a cylindrical graphite sheet capped by hemispherical ends. It has diameter typically around 1 nanometer. The multi-walled CNTs (MWSNTs) are made of several concentric cylinders of graphitic shells with a layer spacing of 0.3-0.4 nm. It tends to have diameter in the range of 2-100 nm. (Merkoci et al. 2009)

2.3 Biopotential electrodes

Biopotential electrodes are used for recording and stimulating the bioelectric phenomena. The bioelectric signals are mainly produced by muscles and nerves due to the migration of ions. The migration of ions generates potential differences at cellular level including the body's outer surface. Each potential can be picked up by placing

electrodes at any two points at the surface of the body and measured with a recording device. A typical cell potential waveform is shown in Figure 2. (Indian Institute of Technology 2010)

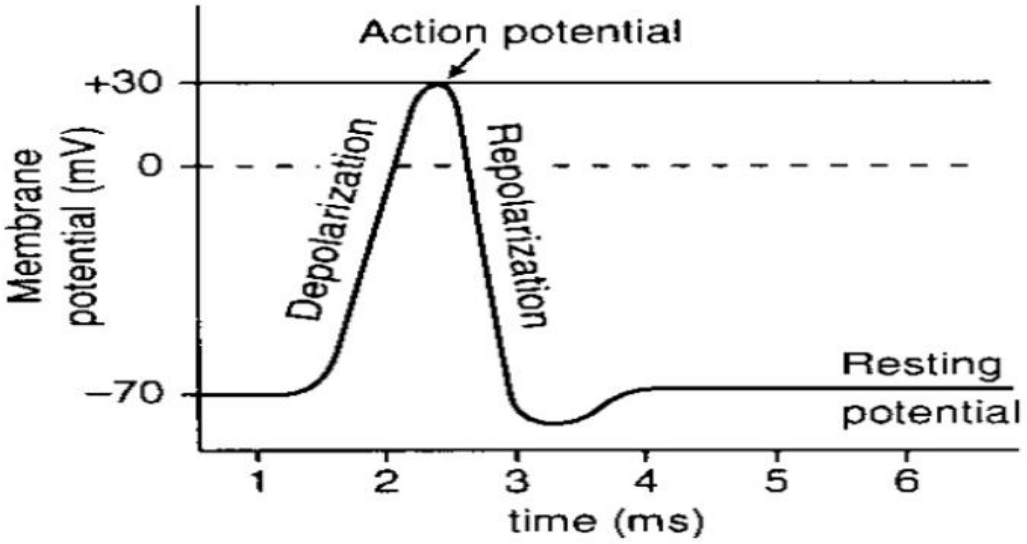

Figure 7: A typical cell potential waveform (Indian Institute of Technology 2010).

When a cell is excited by ionic currents or external stimulus, the membrane potential of a cell changes from its original state. The potential rises due to high influx of sodium ions and reaches the maximum value, which is called action potential. An exciting cell with an action potential is said to be depolarized; this process is called depolarization. After a certain time, the cell becomes polarized and returns back to it's resting potential. This process is known as polarization. After an action potential, there is a period, known as absolute refractory period, in which cell does not respond to any new stimulus. This is followed by a relative refractory period when another action potential may be triggered by a stronger stimulus.

One of the important desirable characteristics of electrodes to pick up these signals is that they should not polarize, meaning that the electrode potential must not vary considerably even when the current is passed through the electrode. Other properties of good electrode includes biocompatibility, good electrical conductivity and corrosion resistance. (Indian Institute of Technology 2010)

2.3.1 Electrode-electrolyte interface

A redox reaction needs to occur at the interface between the electrode and electrolyte for a charge to be transferred between electrode and the ionic solution. A redox reaction is an electrochemical oxidation-reduction reaction. The oxidation is dominant when the current flow is from the electrode to the electrolyte, and the reduction dominate when the current flow is in the opposite. There are two kinds of currents: faradic current due

to the charge transfer through the interface and displacement current arising from the displacement of charge carriers at the interface. The displacement current is also called as capacitive current. (Riistama 2010; Woo 2015) An electrode-electrolyte interface is shown in Figure 3.

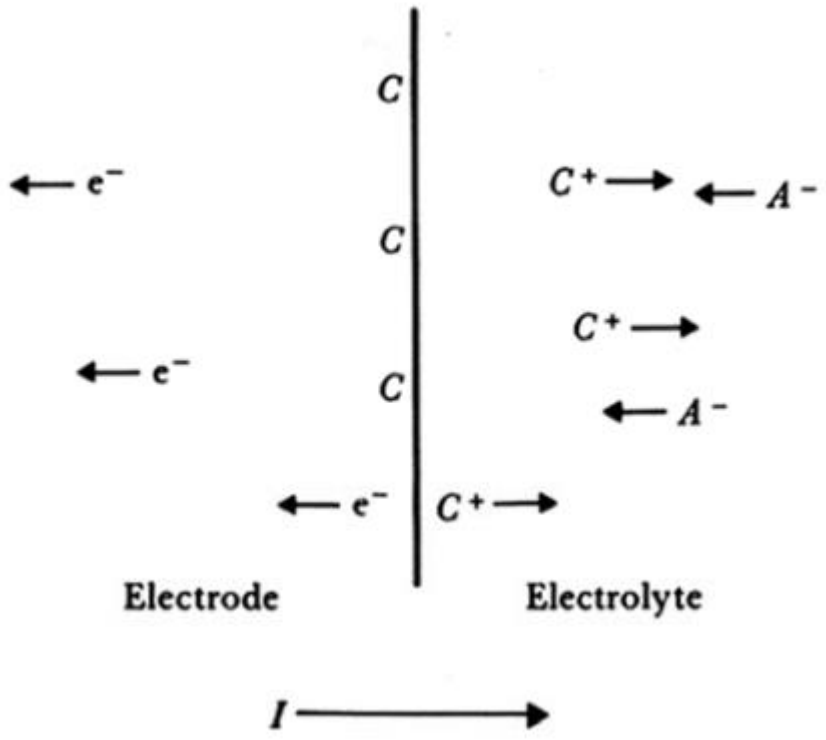

Figure 8: Electrode-electrolyte interface (Woo 2015).

When the metallic atoms of the electrode are oxidized, the reaction can be stated as:

$$C \leftrightarrow C^{n+} + n(e^-) \quad (5)$$

where C represents the metal atom, n its valence, e^- an electron and $n(e^-)$ number of electrodes. When the reduction/oxidation of the electrolyte ions is to occur, the reaction will be written as:

$$A^{n-} \leftrightarrow A + n(e^-) \quad (6)$$

where A^{n-} represents an anion atom or molecule of the electrolyte solution and A is the atom or molecule of the electrolyte.

Thus, the net current crossing the electrode-electrolyte interface are: a) electrons moving in an opposite direction of current, b) cations (C^+) moving in the same direction as current and c) anions (A^-) moving in an opposite direction of current. These redox reaction causes a changes in the charge distribution between the interface and rest of the electrolyte. The charge distribution at the interface can be measured as the higher electrode potential than in the bulk electrolyte. The layer with a high charge density at the interface is called a double layer. (Riistama 2010; Woo 2015)

2.3.2 Electrical characteristics

The electrical characteristics of a biopotential electrode can be represented by RC circuit in Figure 4 below. In the circuit below, C_d is the capacitance across the charge double layer, R_d is the leakage resistance across the charge double layer, R_s is the resistance of electrolyte and E_{hc} is the Dc voltage source or half call potential. R_d and C_d are the impedance associated with the electrode-electrolyte interface and polarization effects. R_s is the series resistance associated with the interface effects and due to resistance in the electrolyte. The value of C_d and R_d changes with frequency, current density, electrode material and electrolyte concentration whereas value of R_s changes with electrolyte concentration. (Woo 2015)

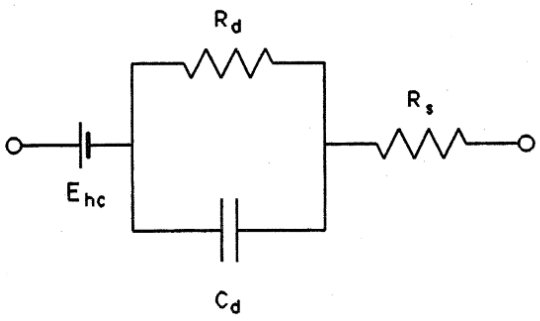

Figure 9: The equivalent circuit for a biopotential electrode in contact with an electrolyte (Woo 2015).

The impedance of the electrode is frequency dependent as show in Figure 5. At low frequencies the impedance is dominated by the series combination of R_s and R_d, whereas, at higher frequencies C_d bypasses the effect of R_d so that impedance is now close to R_s. Thus, it is possible to determine the component values for the equivalent circuit for a electrode by measuring the impedance at high and low frequencies.

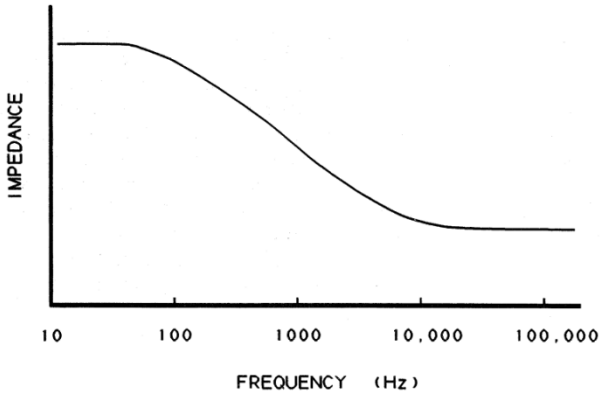

Figure 10: An example of biopotential electrode as a function of frequency (Neuman 2000).

The impedance is characterized by a magnitude (|Z|) and phase angle (Θ) and is most generally represented as a function of frequency. For a capacitor, the impedance is purely imaginary, the phase angle is 90° and the current is out of phase with voltage by 90°. For a resistor, the impedance is real, the current and voltage are in phase and the phase angle is 0°. For a system composed of combination of these components like in the electrical electrode-electrolyte interface, a large phase angle value indicates that the impedance is predominantly capacitive, while small angle values are resistive. (Cui et al. 2001) The electrical characteristics of electrodes are also affected by it's physical properties which is shown in Table 1below. It is seen that the increase in surface area and surface roughness of the electrode decreases the electrode impedance. However, polarization of the electrodes increases the electrode impedance at lower frequencies.

Table 1:The Effect of Electrode Properties on Electrode Impedance (Neuman 2000).

Property	Change in Property	Changes in Electrode Impedance
Surface area	↑	↓
Polarization	↑	↑↓ At low frequencies
Surface roughness	↑	↓

2.3.3 General requirements of the electrode material

The noble metals electrode like platinum(Pt), gold, iridium, palladium and rhodium have been commonly used for electrical stimulation. Their intended application might be different due to their material properties. Platiunum is relatively soft material and may not be mechanically acceptable for all stimulation applications. Iridium is harder than Platinum making it more suitable as intracortical electrodes. (Merrill et al. 2005) Some of the basic requirement criteria of an electrode material are listed in Table 2 below.

Table 2: Basic requirements of an electrode material (Merrill et al. 2005).

Biocompatibility	The electrode material should be biocompatible to avoid a necrotic cell response.
Stable junction	A stable junction should be formed between electrode and tissue, especially in long term in vitro and in vivo measurements.
Mechanical strength	Electrode material should offer sufficient mechanical strength combined with stable electrical properties for reliable long term performance of MEA.
High charge injection capacity	A safe stimulation conditions for reliable stimulation of excitable tissue can be achieved by a sufficient high charge capacity per surface area.
Electrical conductivity	A good electrical conduction between electrode and tissue is crucial for stimulation and recording of bioelectrical signals.
Corrosion resistance	An electrode material should not erode in biological environment when implanted.

2.3.4 Safe charge injection limit and stimulation protocol

The two most important parameters for designing a stimulation protocol is: a) Efficiency and b) safety. An efficient stimulation pulse requires to have a sufficient high charge per pulse whereas a safety pulse requires a sufficient low charge per pulse to prevent electrode corrosion. (Merrill et al.2005) The maximum safe charge that can be injected through a microelectrode depends on several factors including the electrode material, the electrolyte, stimulation parameters (charge per pulse, duration, waveform type, frequency) as well as the shape and size of the electrode. Microelectrodes of small dimensions may safely inject less charge than macroelectrodes, however the efficiency may be compromised in such case. Therefore, sufficient charge injection into the microelectrode often brings the limiting factor for the efficient stimulation of the surrounding tissues with electrodes. One way to overcome this problem is by increasing the effective surface area of the microelectrodes, which decreases the impedance and the thermal noise of the electrode and also allows to inject higher charges, necessary for efficient and reliable stimulation of excitable tissues. (Heim et al. 2012)

The basic design criteria for a safe stimulation protocol can be stated according to Merrill et al.2005 as: "The electrode potential must kept within a potential window where irreversible faradic reactions do not occur at levels that are intolerable to the

physiological system or electrode. If irreversible faradic reactions do occur, one must ensure that they can be tolerated (e.g. that physiological buffering systems can accomodate any toxic products) or that their detrimental effects are low in magnitude (e.g. that corrosion occurs at a very slow rate and the electrode will last for longer than its design lifetime)." Therefore, currents injected into a microelectrode should not exceed a certain safe limit to avoid irreversible faradic reactions at the electrode surface.

2.3.5 Charge vs charge density relationship

According to Shannon (1992),an expression for the maximum safe level for stimulation is given by :

$$\log(Q/A) = k\text{-}\log(Q) \tag{7}$$

where Q is the charge (μC) per phase, Q/A is charge density (μC/cm^2) per phase and 2.0 >k > 1.5, where k is constant which fits to the empirical data findings in the above research(Merrill et al. 2005). Figure 6 illustrates the charge vs charge density relationship of equation (4) using k values of 1.7, 1.85, and 2.0.

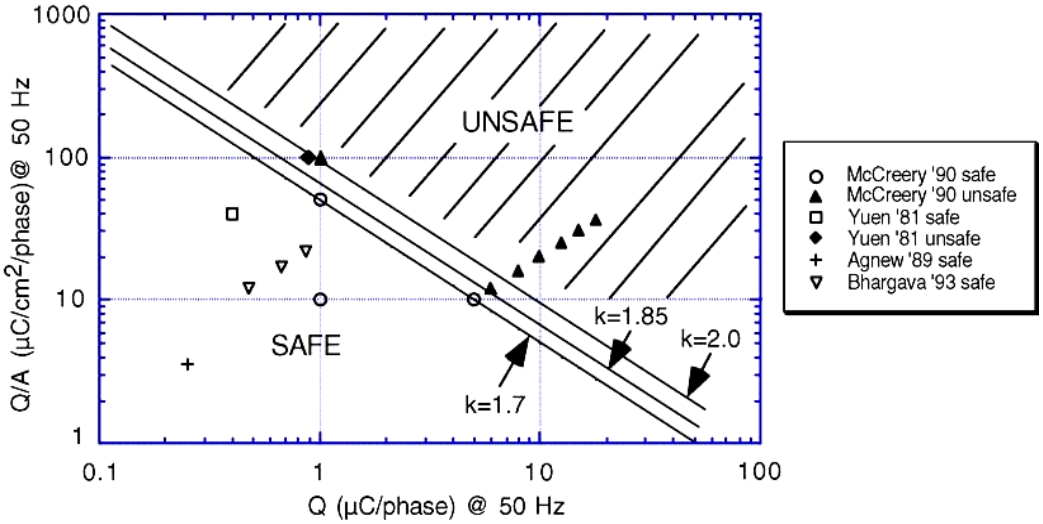

Figure 11: Charge (Q) vs. charge density (Q/A) for safe stimulation at the frequency of 50 Hz. A microelectrode with relatively small total charge per pulse might safely stimulate using a large charge density, whereas a large surface area electrode (with greater total charge per pulse) must use a lower charge density. (Merrill et al. 2005)

The data shows that as the charge per phase increases, the charge density for safe stimulation decreases. Above the threshold for damage, experimental data demonstrates tissue damage, and below the threshold line, the data indicates no damage. When the total charge is small as with a microelectrode, a relatively large charge density may safely be used. It is seen that both charge per phase and charge density are important parameters that determines the neuronal damage to cat cerebral cortex. In terms of the mass action theory of damage, charge per phase determines the total volume within which the neurons are excited, and the charge density determines the proportions of

neurons that are close to an excited electrode. (Merrill et al. 2005) The area of safe stimulation also depends upon the types of tissues stimulated (mass action theory) (McCreery et al.1990). For example, the limits for safe stimulation in deep brain was found to be 30 μC/cm^2 for an injected charge of 2 μC per phase (Kuncel & Grill 2004).

3 MATERIALS AND METHODS

3.1 Material and solution preparation

We used Pyrrole (Py) monomer (Sigma Aldrich, St. Louis, USA)of concentration0.2 M and Dodecyl-benzene sulphonate (DBS) (Acros Organics, Geel, Belgium) concentration of 0.05 M to make the solutions. A (PPy)-DBS solution was made by adding 1.39 ml of Py solution and 1.98 g of DBS to 100 ml of distilled water. We used magnetic stirrer for 30 minutes to achieve homogenous solution. We had single-walled carbon nanotubes (SWCNTs) functionalized with COOH (University of Oulu) of three different concentrations. We used three different concentrations of CNTs: 0.1 mg/ml, 0.25 mg/ml and 0.5 mg/ml of COOH/DI-water. The chemical structures of these chemicals are shown in Figure 7 below.

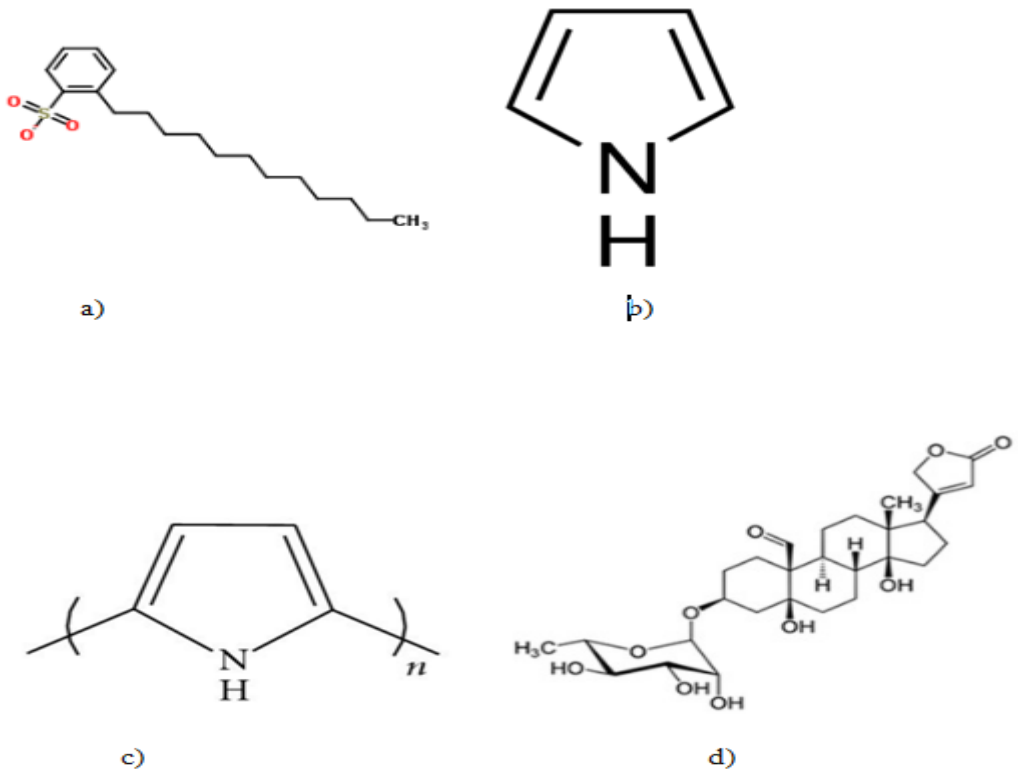

Figure 12: The chemical structures of a) DBS b) Py monomer (Royal Society of Chemistry2015). c) PPy (Chidichimo et al. 2010). d) CNT (C29H42O10, MW 550.64) (Yang et al. 2014).

We used two types of platinum electrodes for the coatings, MEA electrodes and macroelectrodes. MEA electrodes (MEA60 100 Pt, Qwane Biosciences, City, Country) consisted of 60 recording electrodes with a diameter of 30 µm and interelectrode distance of 100 µm. The size of the MEA electrode array is 15mm*15mm*0.7mm.

Each electrode has impedance value of 800-1100KOhm at frequency of 1KHz. Macroelectrode were made of 99.95% Pt with the dimensions of 1.0mm*0.5mm*15 mm (Labor-Platina Kft, Pilisvörösvár, Hungary). We used PPy-DBS and PPy-DBS/CNT solutions for macroelectrode coating while only PPy-DBS solution for MEA electrode coating. The coating solution used for each type of coating is presented in Table 3 below.

Table 3: Electrodes and coating solutions used.

Electrode types	Coating solution
MEA electrodes	PPy-DBS
Macroelectrodes	PPy-DBS PPy-DBS+CNT 0.1mg/ml PPy-DBS+CNT 0.25mg/ml PPy-DBS+CNT 0.5mg/ml

3.2 Polymerization

The electrochemical polymerization was carried out using a potentiostatic step method at a constant voltage in a two-electrode electrochemical cell as shown in Figure 8 below. The coating solution for each electrode types are listed in Table 3. All the electrodes were polymerized by using VersaSTAT Series potentiostat/galvanostat device controlled by VersaStudio software (Princeton Applied Research, South Illinois, USA). We used the linear scan voltammetry and chronopotentiometry technique to generate the current and charge density curves.

We controlled the process by charge limits. The settings for the each electrodeposition are listed in the Results section 3.1 later. The experiment were carried out at room temperature. The data from the software was exported to CView software (Scribner Associates, North Carolina, USA) to further analyze the data.

The electrode to be coated (working electrode) was supplied with certain potential (V) with respect to the reference electrode from the potentiostat and the current (I) was measured from the counter electrode. We used Pt counter electrode of dimesnions 1.0mm*0.5mm*15 mm (Labor-Platina Kft, Pilisvörösvár, Hungary). We used 12ml of

solution for macroelelectrode coating and 2ml for microelectrodes coating. The values of currents, voltages and times are given in Result section later.

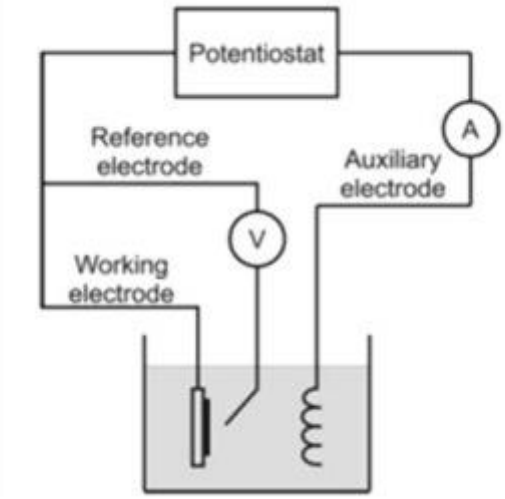

Figure 13: Electrochemical cell setup (Li & J 2010).

3.3 Impedance measurement

We used two devices for the impedance measurement. The MEA electrodes impedance was measured with Impedance testing device MEA-IT (Multi Channel Systems, Reutlingen, Germany). The macroelectrodes were measured with Solartron Model 1260A Frequency Response Analyzer in combination with 1294A Impedance Interface and SMaRT Impedance Measurement Software (Solartron Analytical, Hampshire, UK).

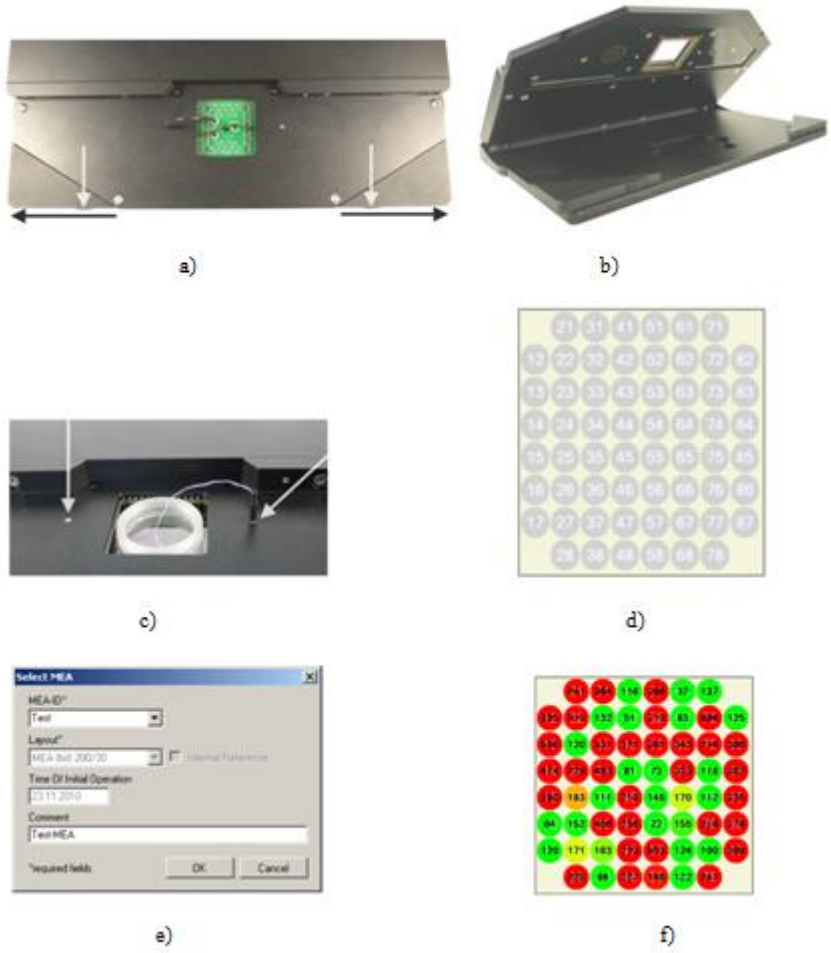

Figure 14: a) Mounting the MEA electrodes b) MEA-IT device and c) Ag-Agcl silver wire ground electrode d) Virtual MEA layout e) Measurement with MEA-IT software and f) Measured electrode impedance (Impedance Testing Device MEA-IT Manual2013).

First we carefully inserted the MEA in the middle of the lid as shown in Fig 9 a) making sure that it is correctly oriented. Then, we filled the MEA dish with a conducting Phosphate Buffered saline (PBS) solution (Sigma Aldrich, St. Louis, USA) and approximately fifteen minutes was waited before measuring the electrodes. At the same time, we externally grounded Ag-Agcl silver wire even though we measure a MEA with internal reference electrode as seen in Fig 9 c). Otherwise the impedance values would be out of range. We used MEA-IT software (Multi Channel Systems, Reutlingen ,Germany) to control the impedance measurement as seen in Figure 9.

3.3.1 Macroelectrode impedance measurement

We used Solartron Model 1260A Frequency Response Analyzer, 1294A Impedance Interface and computer equipped with the SMaRT Impedance Measurement Software (Solartron Analytical, Hampshire, UK) to measure the impedance.

We used three-electrochemical cell setup for impedance measurement as shown in Figure 10 below. We used MF-2052 RE-5B Ag/AgCl reference electrode with flexible connector (Labor-Platina Kft, Pilisvörösvár, Hungary), Pt as a counter electrode and Pt sample as a working electrode. The potential (V) was supplied between reference and working electrode and the current flow between WE and CE was measured. We used 10ml PBS solutions as electrochemical solution. The dc level voltage and ac voltage were set to 0V to 5mV, respectively. Impedance was measured at 26 discrete frequency points from 1.0 Hz to 100 000 Hz using frequency sweep option. These measurements were analyzed by using Smart v3.2.1 software (Solartron Analytical, Hampshire, UK) and Microsoft Excel (Microsoft, Washington, USA).

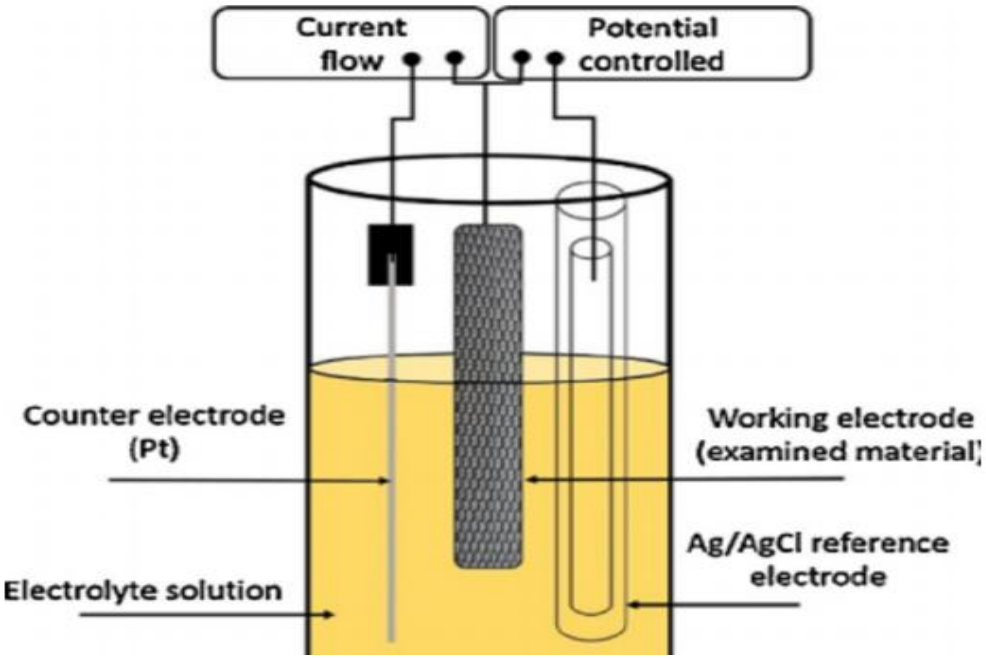

Figure 15: Three-electrode electrochemical setup (Ayoub et al. 2016).

3.4 Imaging device

We used Wyko NT1100 Optical Profilometer, (Veeco, City, Country), Park XE-100AFM Atomic Force Microscopy (Park Systems, Santa Clara, USA), and Olympus BH-2Optical microscope (Olympus Optical Co., Tokyo, Japan) equipped with a BestScope BUC4-500C5.0 MP digital camera (BestScope International Limited, Beijing, China) to capture the images of the coated electrodes.

3.4.1 Optical Profilometer

We used Wyko NT1100 Optical Profilometer to capture the 3D image of macroelectrodes. The basic principle and the measurement of the device is described below in Fig 11 and Fig 12 respectively.

3.4.1.1 Principle

Optical Profilometer uses the wave properties of light to compare the optical path difference between a test surface and a reference surface. A light beam is split, reflecting half the beam from a test material which is passed through the focal plane of microscope objective, and the other half of the split beam is reflected from the reference mirror. Interference occur in the combined beam wherever the length of the light beams vary. The interference beam is focused into a digital camera to create light and dark interference image as shown in Figure 11 below. With a known wavelength, the height differences across a surface is calculated. From these height differences, a surface 3D map is obtained. (Zygo Corportion 2017)

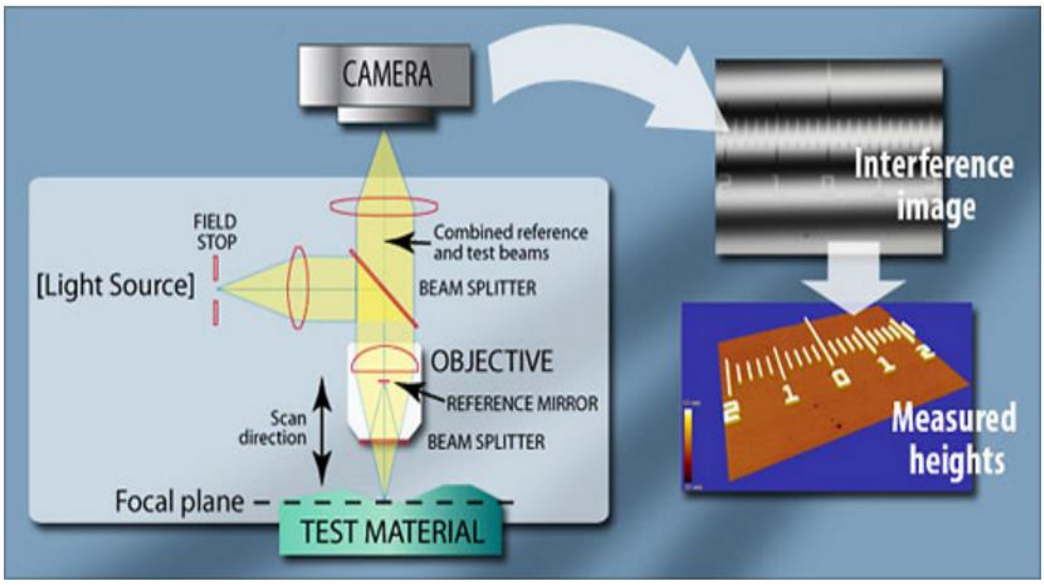

Figure 16: Schematic of an optical profilometer (Zygo Corportion 2017).

3.4.1.2 Measurement

First of all, the profilometer was calibrated in Vertical Scanning Interferometry (VSI) measurement mode with VSI calibration sample as shown in Figure 12 below. The sample was mounted on the Profilometer stage and the program was started by double clicking the Vision64 software icon, to open the calibration mode. We selected the filter to VSI mode and adjusted the intensity and focus with the slider in the computer window. The illumination was increased until we see red on the screen and decreased the illumination until the red was un-illuminated. Then the calibration sample was focused by rotating the focus Knob slowly until we get the good contrast image of the sample. Then, we repeated the process with the Pt samples and the images were saved in a suitable format.

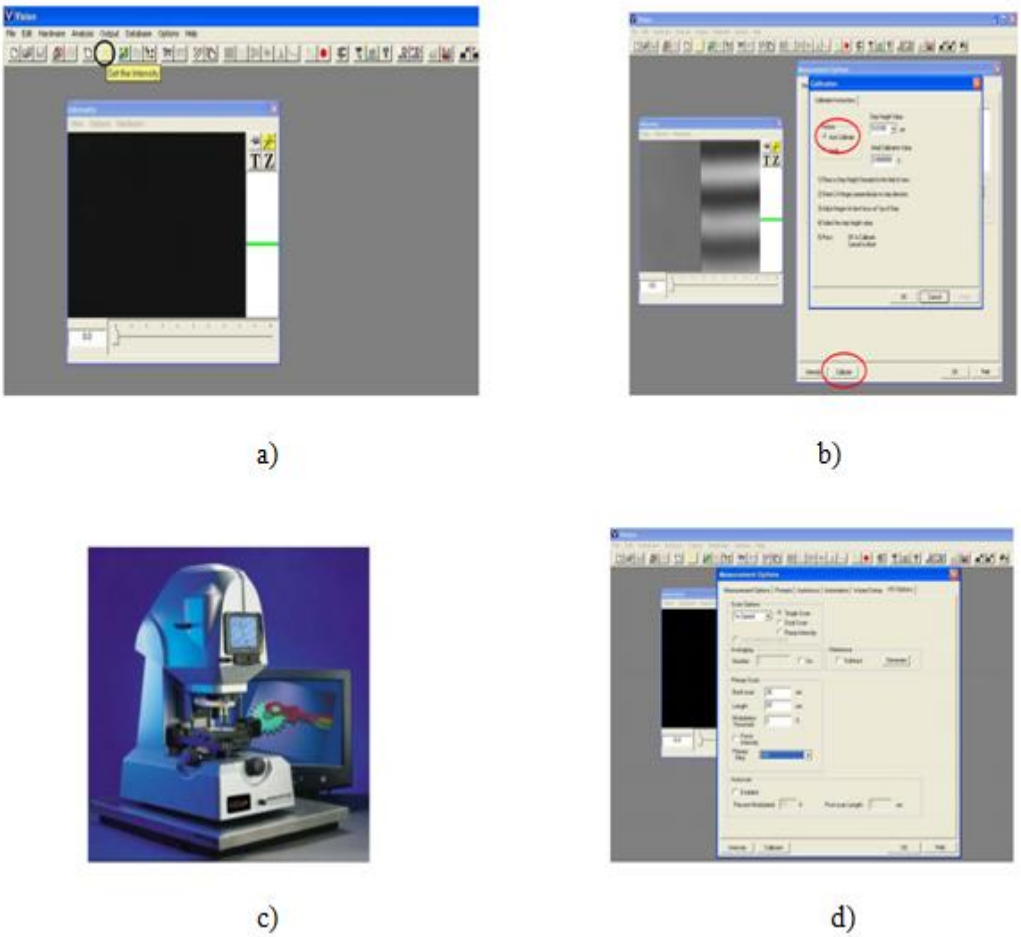

Figure 17: Measurement with Optical Profilometer Vision software with intensity window a), Calibration window b), Veeco NT1100 c) and Measurement option window d) (Marcel 2003).

3.4.2 Atomic Force Microscopy (AFM)

We used Park XE-100AFM Atomic Force Microscope, to image the surface topography of coated electrode. We calculated the peak-to-valley roughness index(Ra) of the image using the vertical height of the image surface (The Research membranes Environment, 2009) in Figure 26 below in the Results section. The basic measurement and hardware setup are shown below in Figure 13 and Figure 14, respectively.

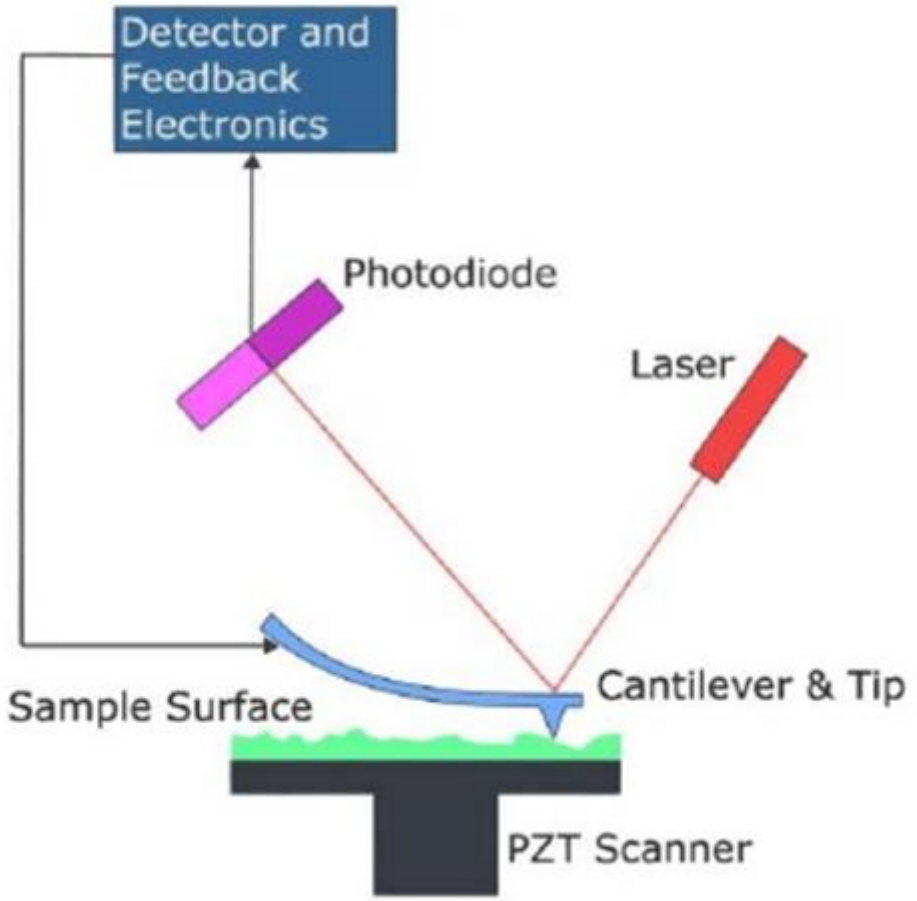

Figure 18: Basic AFM principle (Stonecypher 2011).

3.4.2.1 Principle

An AFM uses a cantilever tip to scan over a sample surface. As the tip approaches the surface, attractive forces between the tip and surface causes the cantilever to deflect towards the surface. However, if the tip makes contact with the surface, repulsive force takes over and causes the cantilever to deflect away from the surface. A laser beam is used to detect deflections away or towards from the surface. A deflection in the cantilever causes the changes in the direction of the reflected beam. The photodiode can be used to measure these changes and thus the topography of the sample image can be created with feedback and electronic circuits. (Stonecypher 2011)

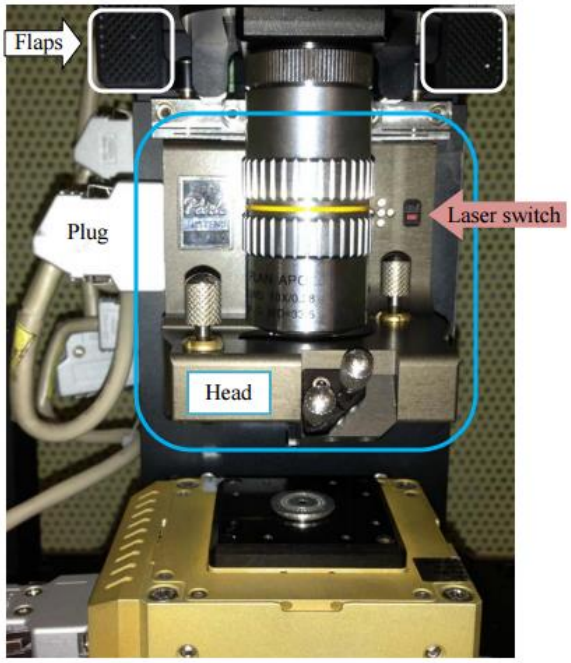

Figure 19: Basic hardware setup of Park XE-100 AFM (Fei & Brock 2013).

3.4.2.2 Measurement

First we mounted sample on the stage and rested the tips in the tips box and that bearings fits into tip slots. Then we replaced head and pushed flaps away until slightly tight. Then after, we checked the Scanning probe mcroscopy (SPM) Controller and Monitors. We turned on the Light Bank, isolation stage and Laser light. After that, we processed the image with 'XEC' program and saved it. (Fei & Brock 2013)

3.4.3 Optical Microscope

Olympus BH-2Optical microscope (equipped with a BestScope BUC4-500C, 5.0 MPdigital camera) was used to capture the mircographs image. The micrographs were taken at 5X, 10x and 20x magnifications.

4 RESULTS

4.1 MACROELECTRODES

The macroelectrodes were successfully electrodeposited with PPy and PPy/CNT solutions. The electrodeposited electrodes are: PPy-Control, PPy-CNT 0.1, PPy-CNT 0.25 and PPy-CNT 0.5. Their impedances were measured using Electrical Impedance Spectroscopy and the images were analysed with AFM, Optical Profilometer and Optical Microscope. The electrodeposition results are presented in section 4.1.1. The Electrical Impedance Spectroscopy and impedance measurement results are presented in section 4.1.2 to 4.1.4. The imaging results are presented in section 4.1.5.

4.1.1 Macroelectrode electrodeposition

All electrodes were polymerized using chronopotentiometry method with a reference potential of 1.0 V. We used charge limit of 0.258C/cm^2 and electrode area of 0.15cm^2 for electrodeposition. The electrodes were successfully polymerized with PPy and combination of PPy and CNT solutions. All the electrodes showed almost similar charge and current density values. The results looked more consistent in each coating than with the microelectrodes plates. PPy-CNT 0.25 showed the maximum current density of 0.0023A/cm^2 as seen in Figure 15 below. All the current density curves reached the peak and then decreased within a second after the deposition process. After a period of some seconds, all the current density curves decreased at constant value of 0.002A/cm^2.

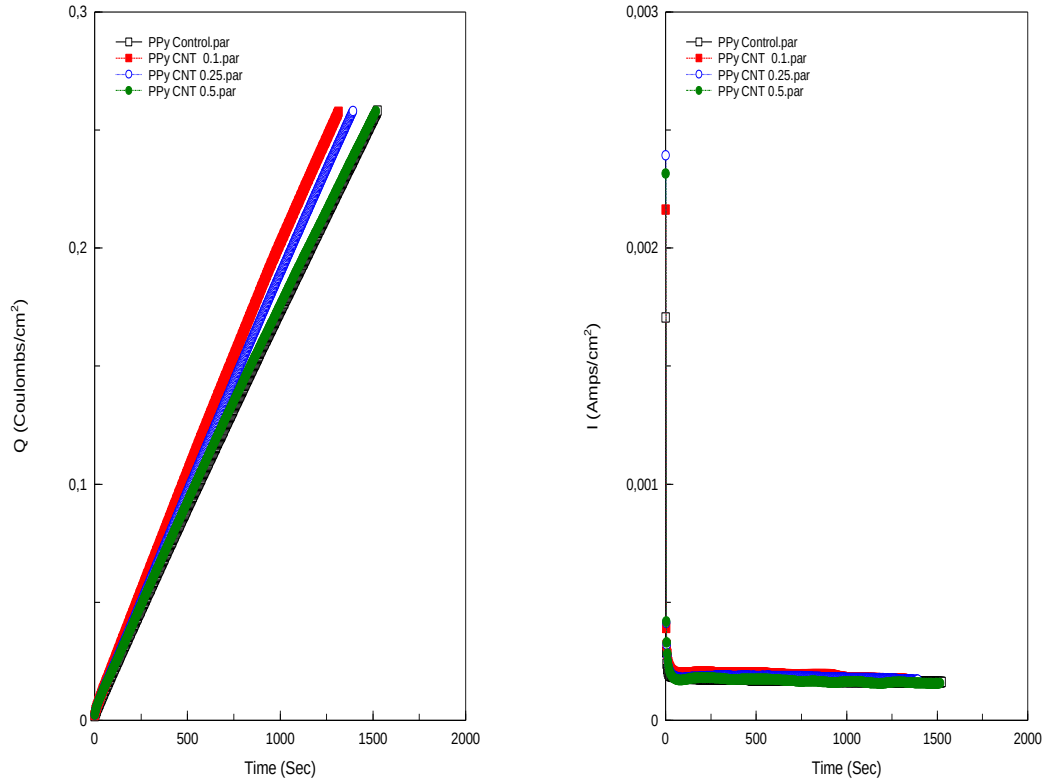

a) b)

Figure 20: Charge a) and current b) densities during electrodeposition.

All the coated platinum samples showed linear increase in charge density as in fig a). Also PPy-Control and PPy-CNT 0.5 showed almost similar response and had a higher time duration of about 1500sec than PPy-CNT 0.1 and PPy-CNT 0.25 samples. No major difference was seen in the current curve as in fig b). PPy-CNT 0.25 showed maximum current density within a few seconds of the electrodeposition process.

4.1.2 Electrical Impedance Spectroscopy

Figure 16 below shows the average bode plot measurements of various samples. PPy-CNT 0.25 showed the highest impedance magnitude while PPy-CNT 0.5 showed lowest value upto frequency of 100Hz. However, the values were very closer after frequency of 100Hz. Bare Pt samples had the highest negative phase angle value upto a frequency of 900 Hz. After this frequency, PPy-CNT 0.25 showed highest negative values. PPy-CNT 0.5 showed least negative phase angle after a frequency of 300Hz. It is seen that the average Bare Pt samples had a dominant capacitive impedance until a frequency of

around 300Hz after which PPy-CNT 0.25 was more capacitive. The electrode impedance was reduced with PPy/CNT composition at lower frequencies, however,PPy-CNT 0.25 was an exception.

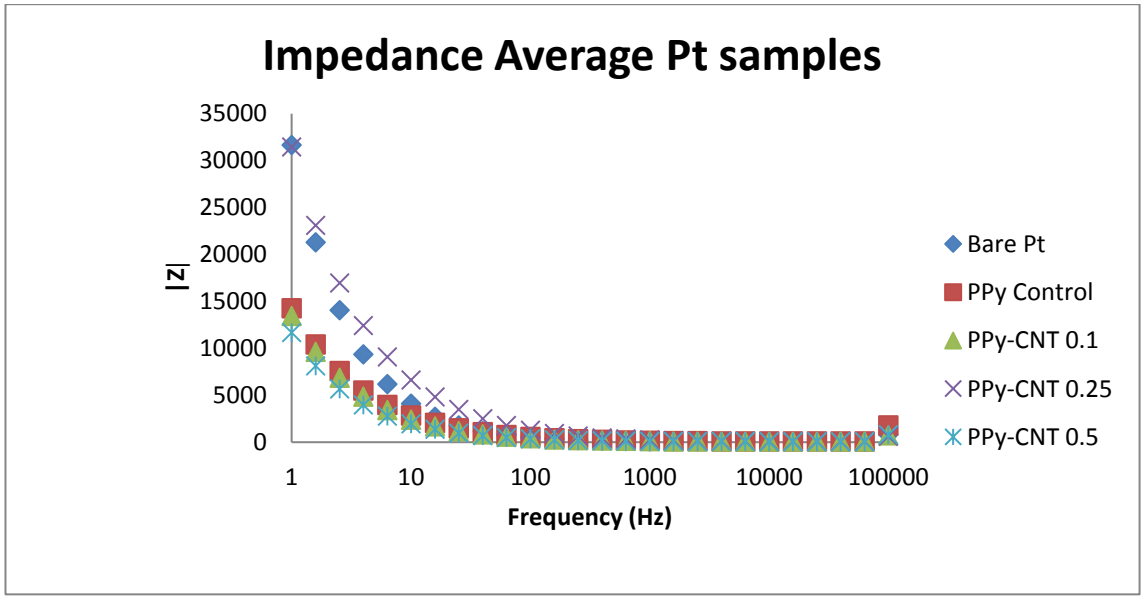

a)

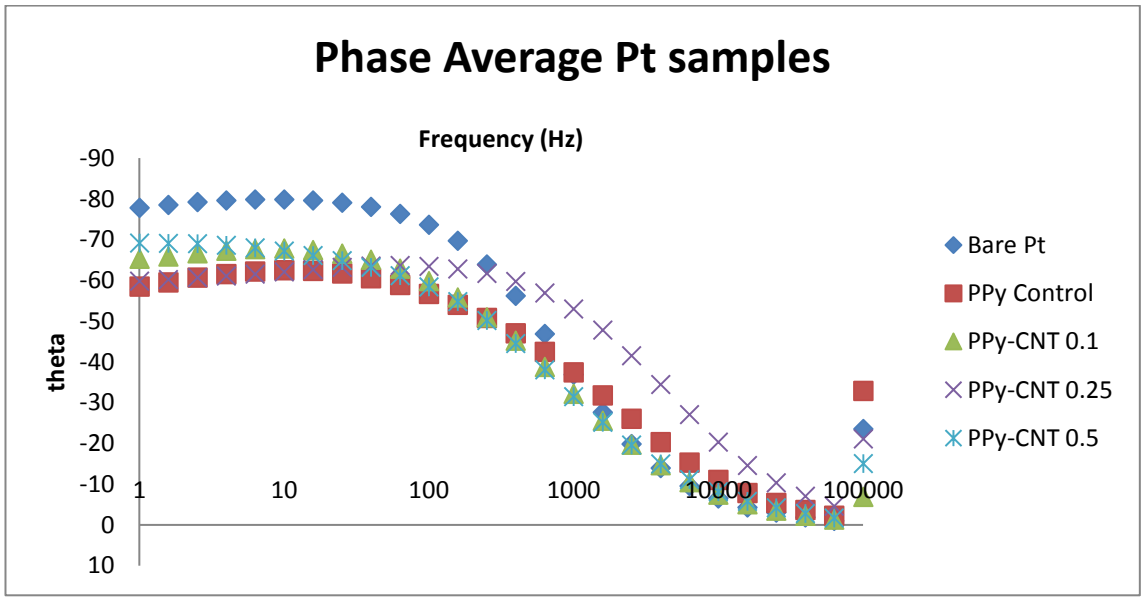

b)

Figure 21: a) Average Bode plot of different Pt samples Impedance plot a) and phase plot b).

At low frequencies (upto 100Hz) bare Pt and PPy-Control 0.25 showed dominant impedance than any other electrodes. However, the values looked similar after 100Hz as seen in Figure 16 a). They also showed a dominant phase angle values at certain range of frequencies which can be clearly noticed from Figure 16 b). The impedance of the individual sample were measured three times to observe the difference in their results as shown in Figure 17, 18, 19, 20 and 21 below. All the measurement samples showed quite similar changes in impedance magnitude and phase. However, PPy-Control and PPy-CNT 0.1 samples showed more variation in their measurement in terms of phase and impedance values respectively.

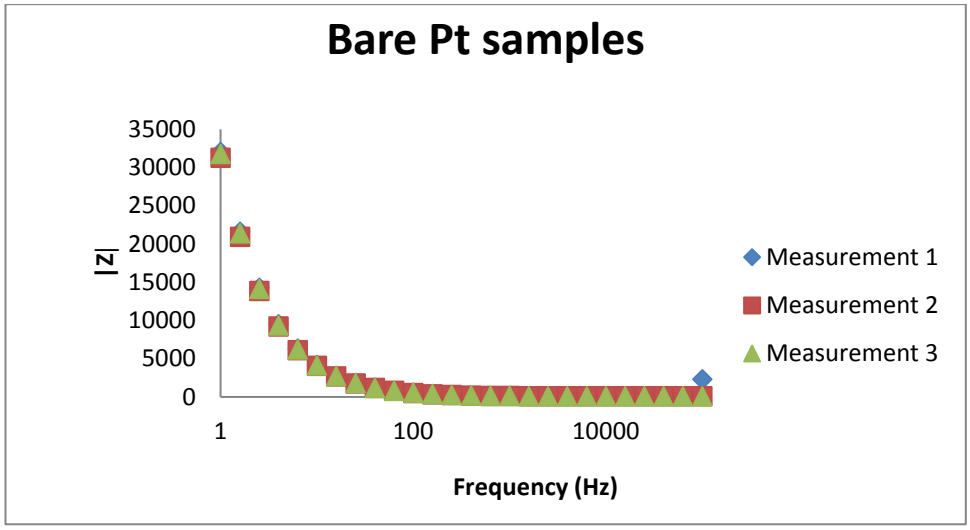

a)

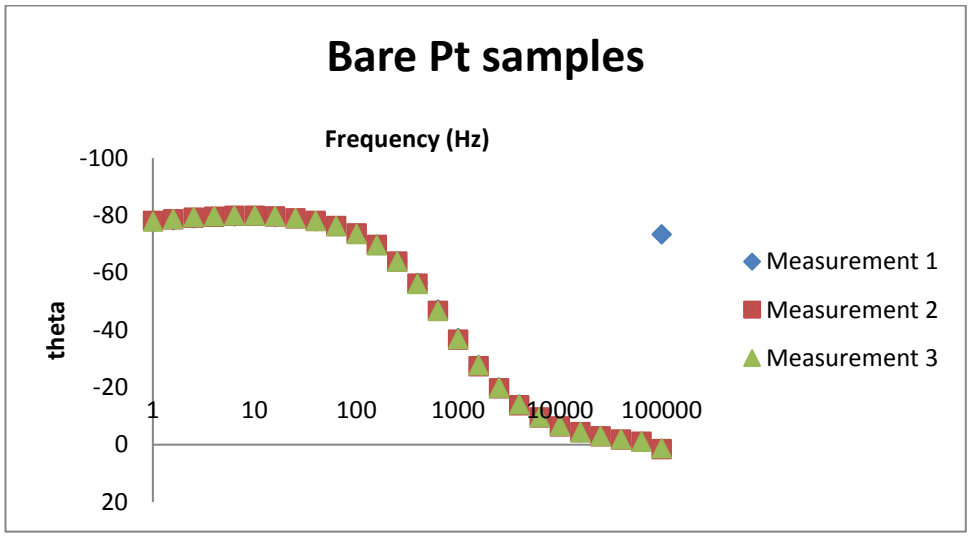

b)

Figure 22: Bode plot of bare Pt sample measured three different times Impedance plot a) and phase plot b) as a function of frequency.

No major difference in the measurement was seen either from impedance magnitude or phase plot. The maximum impedance magnitude of bare Pt sample was around 32000Ohm at the frequency of 1.0Hz. A sharp decrease in impedance magnitude was then observed until the frequency of the 90Hz. The value at this frequency was around 350 Ohm. The values looked consistent after this frequency. The maximum phase angle was around -80°. The phase angle showed almost all similar values until the frequency of 90Hz. After this frequency, the phase angle sharply decreased until the frequency about around 9000Hz. After this frequency, the variation in phase angle values was slower.

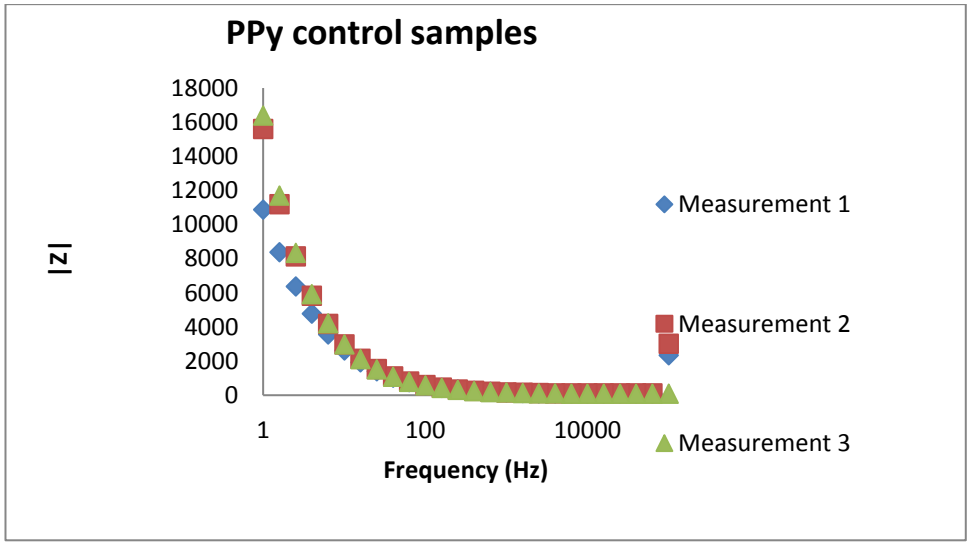

a)

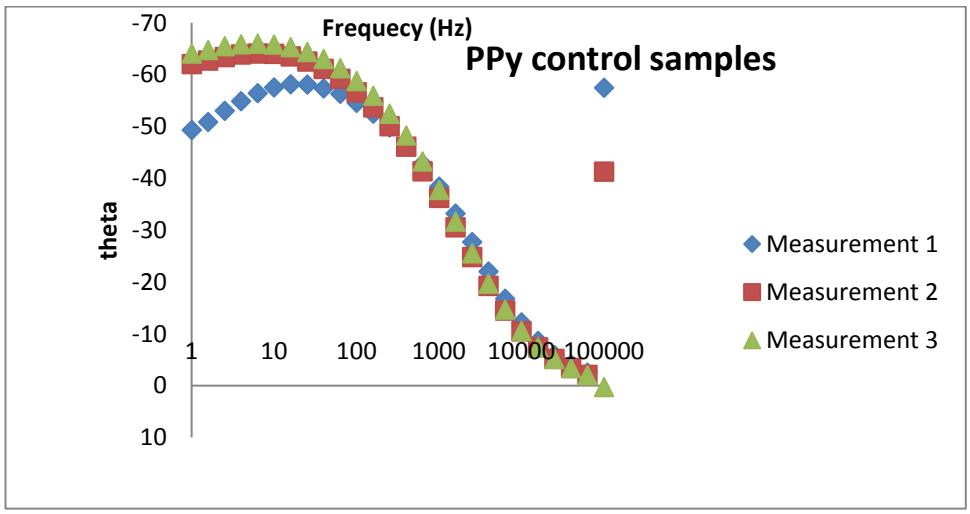

b)

Figure 23: Bode plot of PPy-Control sample measured three different times Impedance plot a) and phase plot b) as a function of frequency.

The maximum impedance magnitude of PPy-Control sample was around 16400Ohm at the frequency of 1.0Hz. A sharp decrease in impedance magnitude was then observed until the frequency of the 90Hz. The value at this frequency was around 560 Ohm. The values looked consistent after this frequency. The maximum phase angle was around -60°. The phase angle showed almost all similar values until the frequency of 90Hz. After this frequency, the phase angle sharply decreased until the frequency about around 9000Hz. After this frequency, the variation in phase angle values was slower.

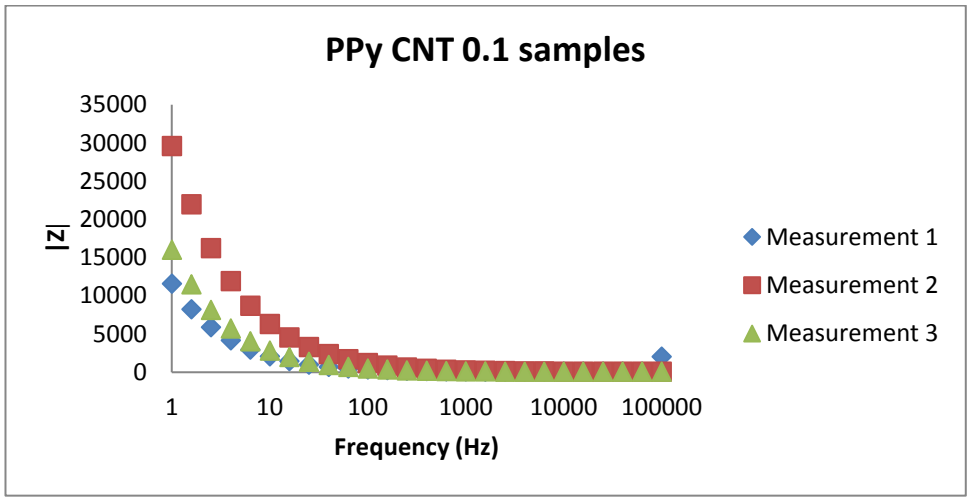

a)

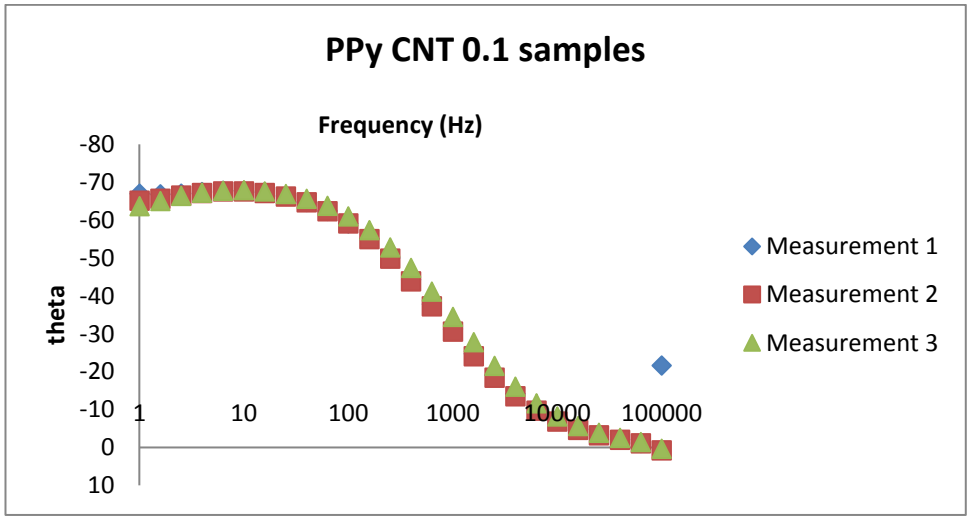

b)

Figure 24: Bode plot of PPy-CNT 0.1 sample measured three different times Impedance plot a) and phase plot b) as a function of frequency.

.No major difference in phase angle measurement was seen from fig b). However, variation of impedance magnitude during the measurement was seen at lower frequencies as in fig a).

The maximum impedance magnitude of PPy-CNT 0.1 electrode was around 16000Ohm at the frequency of 1.0Hz. A sharp decrease in impedance magnitude was then observed until the frequency of the 90Hz. The value at this frequency was around 520Ohm. The values looked consistent after this frequency. The maximum phase angle was around -70°. The phase angle showed almost all similar values until the frequency of 90Hz. After this frequency, the phase angle sharply decreased until the frequency about around 9000Hz. After this frequency, the variation in phase angle values was slower.

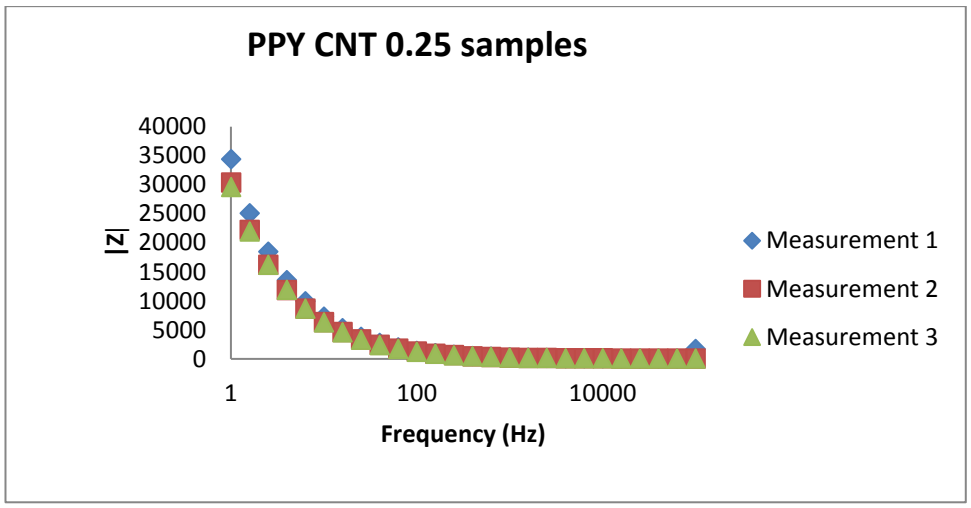

a)

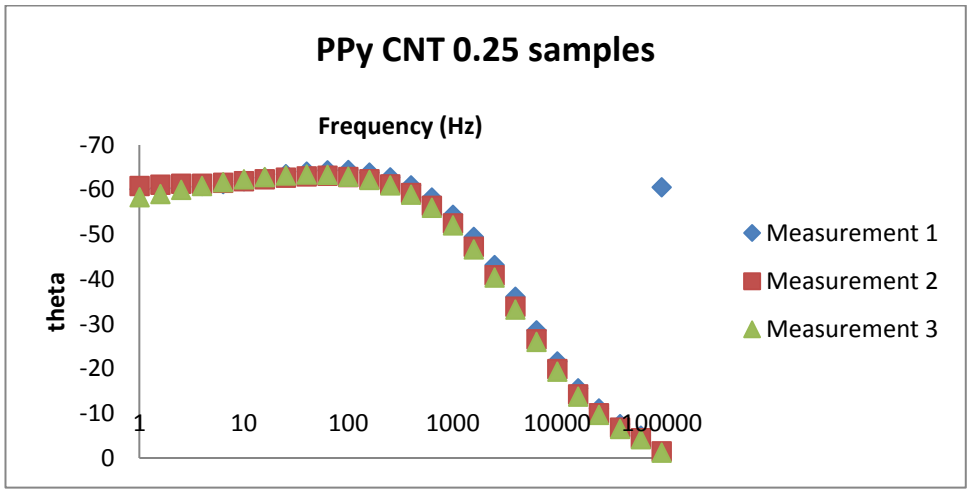

b)

Figure 25: Bode plot of PPy-CNT 0.25 sample measured three different times Impedance plot a) and phase plot b) as a function of frequency.

The maximum impedance magnitude of PPy-CNT 0.25 electrode was around 34400Ohm at the frequency of 1.0Hz. A sharp decrease in impedance magnitude was then observed until the frequency of the 90Hz. The value at this frequency was around 550 Ohm. The values looked consistent after this frequency. The maximum phase angle was around -60°. The phase angle showed almost all similar values until the frequency of 90Hz. After this frequency, the phase angle sharply decreased until the frequency about around 9000Hz. After this frequency, the variation in phase angle values was slower.

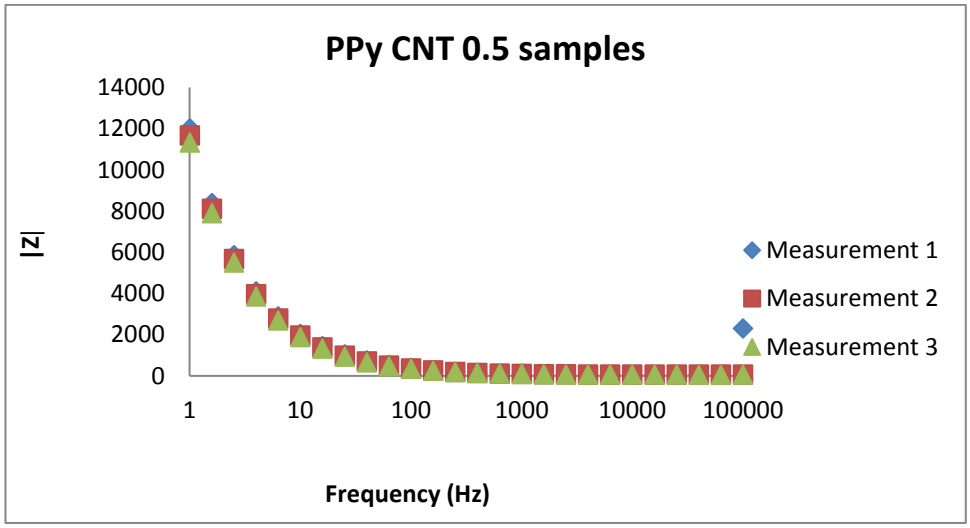

a)

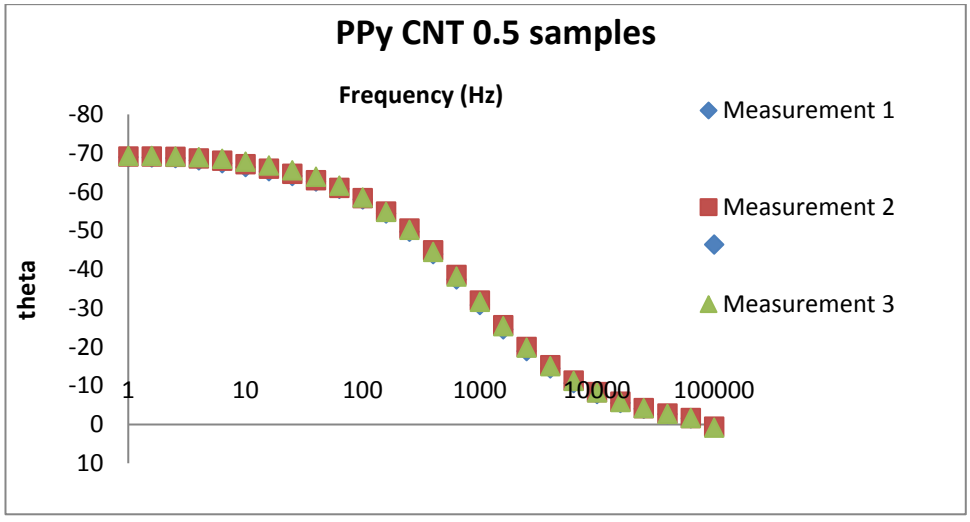

b)

Figure 26: Bode plot of PPy-CNT 0.5 sample measured three different times Impedance plot a) and phase plot b) as a function of frequency.

No variation in the impedance magnitude and phase angle was seen in Fig a) and b). The maximum impedance magnitude of PPy-CNT 0.5 electrode was around 12000Ohm at the frequency of 1Hz. A sharp decrease in impedance magnitude was then observed until the frequency of the 90Hz. The value at this frequency was around 200 Ohm. The values looked consistent after this frequency. The maximum phase angle was around -70°. The phase angle showed almost all similar values until the frequency of 90Hz. After this frequency, the phase angle sharply decreased until the frequency about around 9000Hz. After this frequency, the variation in phase angle values was slower.

4.1.3 Impedance measurement at frequencies of 1Hz and 1kHz

The impedance measurement of different electrodes were done three times. M1 means the first measurement and so on. The measurement values of the samples: Bare Pt, PPy-Control, PPy-CNT 0.1, PPy-CNT 0.25 and PPy-CNT 0.5 is shown in Table 4 below.

Table 4: Impedance magnitude and phase of different electrodes at 1.0Hz and 1000Hz.

Frequency(Hz)	Impedance magnitude(Ohm)			Phase (Θ°)		
Bare Pt	M1	M2	M3	M1	M2	M3
1.0	32000	31250	31760	-80	-80	-80
1000	110	100	100	-40	-40	-40
PPy-Control	M1	M2	M3	M1	M2	M3
1.0	10900	15600	16400	-60	-60	-60
1000	160	170	150	-40	-40	-40
PPy-CNT 0.1	M1	M2	M3	M1	M2	M3
1.0	11600	12800	16000	-70	-70	-70
1000	100	120	130	-30	-30	-30
PPy-CNT 0.25	M1	M2	M3	M1	M2	M3
1.0	34400	30380	29600	-60	-60	-60
1000	270	250	240	-60	-50	-50
PPy-CNT 0.5	M1	M2	M3	M1	M2	M3
1.0	12000	11700	11340	-70	-70	-70
1000	120	110	100	-40	-40	-40

The maximum impedance magnitude for bare Pt electrode was around 32000Ohm at the first measurement at frequency of 1.0Hz, the while all the phase angle was equal to around -80°. Similarly, the maximum magnitude at 1000Hz was around 110Ohm and all the phase angle was equal to around -40°. The least magnitude at 1.0Hz and 1000Hz was around 31250Ohm and 100Ohm respectively.

The maximum impedance magnitude for PPy-Control electrode was around 16400Ohm at the third measurement at frequency of 1.0Hz, the while all the phase angle was equal to around -60°. Similarly, the maximum magnitude at 1000Hz was around 170Ohm and all the phase angle was equal to around -40°. The least magnitude at 1.0Hz and 1000Hz was around 10900Ohm and 150Ohm respectively.

The maximum impedance magnitude for PPy-CNT 0.1 electrode was around 16000Ohm at the third measurement at frequency of 1.0Hz, the while all the phase

angle was equal to around -60°. Similarly, the maximum magnitude at 1000Hz was around 130Ohm and all the phase angle was equal to around -40°. The least magnitude at 1.0Hz and 1000Hz was around 11600Ohm and 100Ohm respectively.

The maximum impedance magnitude for PPy-CNT 0.25 electrode was around 34000Ohm at the first measurement at frequency of 1.0Hz, the while all the phase angle was equal to around -60°. Similarly, the maximum magnitude at 1000Hz was around 270Ohm and all the phase angle was equal to around -50°. The least magnitude at 1.0Hz and 1000Hz was around 29600Ohm and 240Ohm respectively.

The maximum impedance magnitude for PPy-CNT 0.5 electrode was around 12000Ohm at the first measurement at frequency of 1.0Hz, the while all the phase angle was equal to around -70°. Similarly, the maximum magnitude at 1000Hz was around 120Ohm and all the phase angle was equal to around -40°. The least magnitude at 1.0Hz and 1000Hz was around 11340Ohm and 100Ohm respectively.

4.1.4 Average measurement at 1.0Hz and 1.0kHz

The PPy-CNT 0.25 showed highest negative phase angle of 60° at frequency of 1.0kHz while PPy-CNT 0.1 showed least negative value of -30°. PPy-CNT 0.25 also showed least negative phase angle of -58° at 1.0Hz while bare Pt showed highest negative value of -80°. This shows that PPy-CNT 0.1 was highly resistive at 1.0kHz while bare Pt was highly capacitive at 1.0Hz.

Bare Pt showed high impedance values at 1Hz and least magnitude at 1.0kHz compared to coated electrodes. PPy-CNT 0.25 showed maximum magnitude at 1.0Hz and PPy-CNT 0.5 showed least magnitude at 1.0kHz. The average impedance and phase were taken from the different measurement of the samples as shown in Fig 22 below at frequency of 1.0Hz and 1.0kHz. The frequency Figure 22 below shows the average values at 1.0Hz and 1.0kHz. PPy-CNT 0.25 showed highest impedance magnitude while PPy-CNT 0.5 showed lowest among the coated samples. Also PPy-CNT 0.5 showed lowest standard deviation compared to other coated samples at both frequencies. The average impedance measured for both bare Pt and PPy-CNT 0.25 was around 3200Ohm while for PPy-CNT 0.5 was around 1200Ohm at frequency of 1.0Hz. PPy-Control and PPy-CNT 0.1 showed the difference of around 200Ohm at 1.0Hz. PPy-CNT 0.25 showed highest impedance magnitude of around 90Ohm while PPy-CNT 0.5 showed lowest with around 60Ohm at frequency of 1.0kHz.

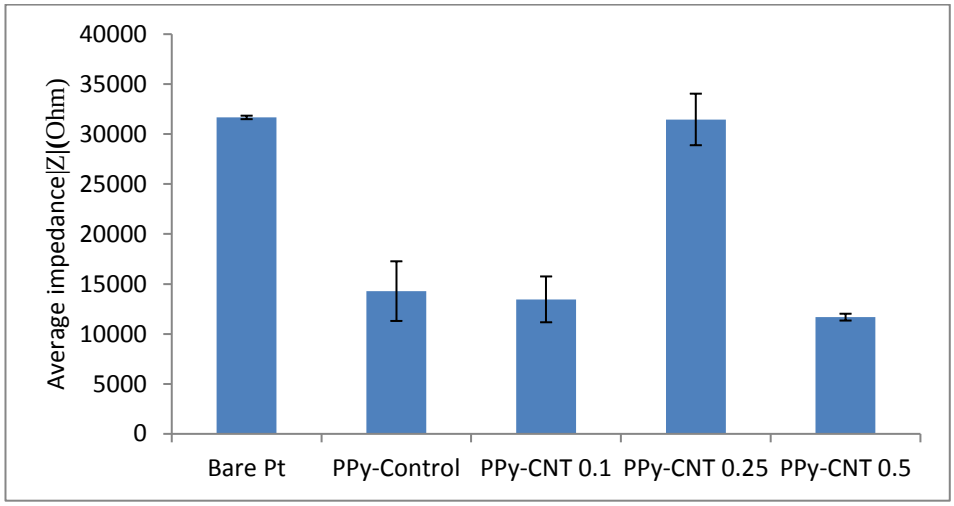

a)At 1.0Hz

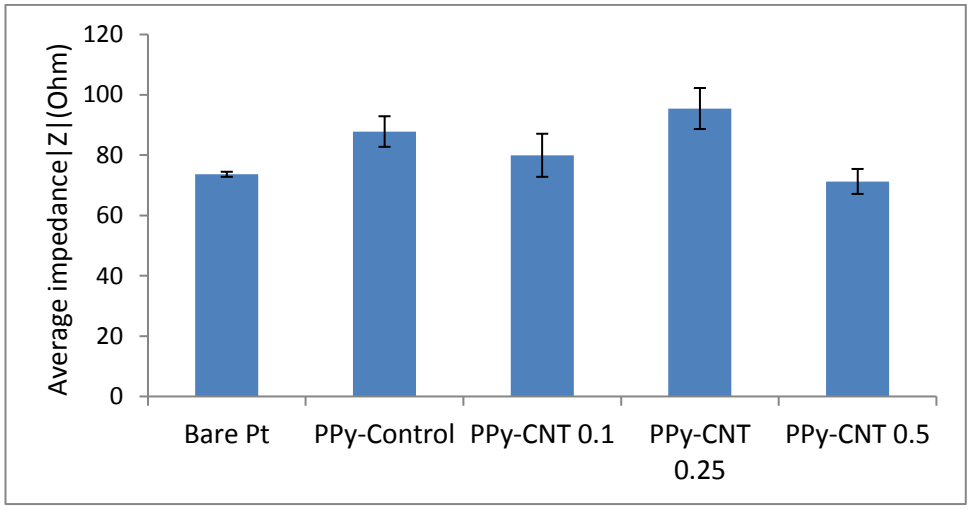

b)At 1.0kHz

Figure 27: Average impedance magnitude of different samples at 1.0 Hz a) and at 1.0 kHz b).

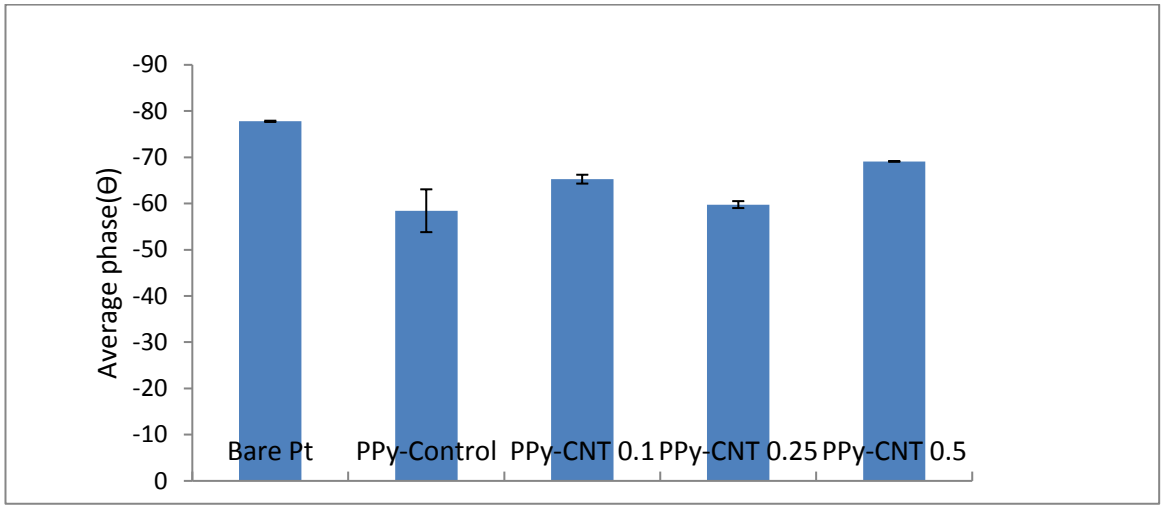

a)At 1.0Hz

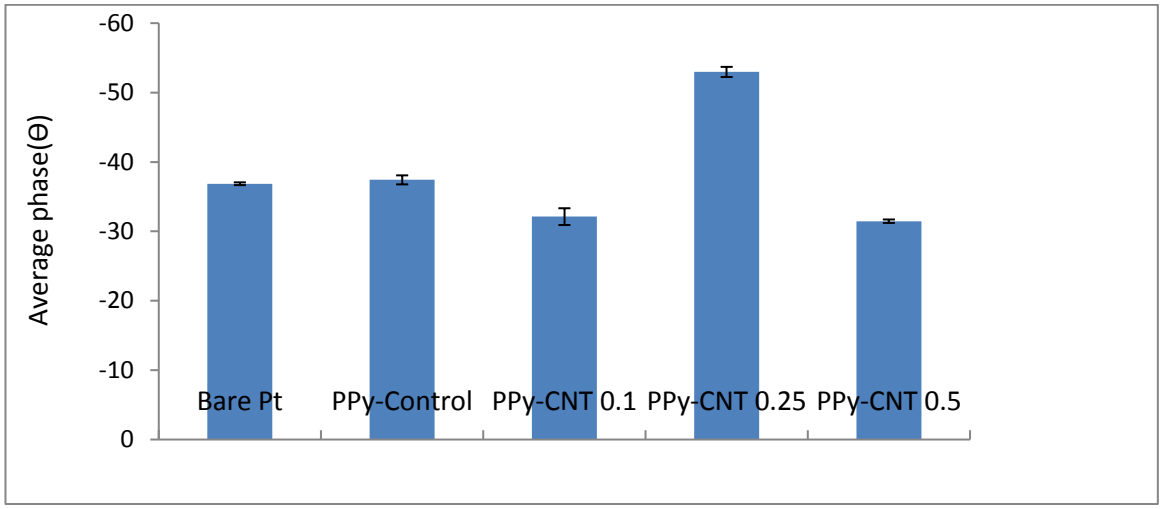

b)At 1.0kHz

Figure 28: Average phase of different samples at 1.0 Hz a) and at 1.0 kHz b).

Bare Pt showed highest phase angle value at 1.0Hz and PPy-CNT showed least value at 1.0kHz compared to coated electrodes. PPy-Control showed least phase angle at 1.0Hz and PPy-CNT 0.5 showed least angle at 1.0kHz. From the Figure above, PPy-CNT 0.5 showed highest negative phase angle of around -70° with least standard error while PPy-control showed least negative phase angle of around -50° with the highest standard error among all the samples as shown in Figure 23. PPy-CNT 0.25 showed the most negative phase angle of around 50° while PPy-CNT 0.5 showed lowest value around -30° with least standard error among all the samples at frequency of 1.0kHz. This suggests that PPy-CNT 0.5 had most resistive impedance at 1.0kHz and most capacitive impedance (compared to other coated electrode) at 1.0Hz.

4.1.5 Surface characterization

The surface morphology of the coated Pt macroelectrode samples were analysed by using AFM, Optical Profilometer and Optical microscope. We calculated the surface roughness from AFM and Optical Profilometer. We observed the coating with the Optical microscope at different magnifications.

4.1.5.1 AFM imaging

The surface roughness of the coated electrodes were measured by using Park XE-100AFM as shown in Figure 24 below. The AFM imaging was conducted on two electrode types: PPy-control and PPy-CNT 0.5. The calculated value of Ra for PPy-Control sample was 1.2µm while Ra for PPy-CNT 0.5 was 5µm. The higher value of Ra showed that the PPy-CNT 0.5 was more rougher than the PPy-Control surface.

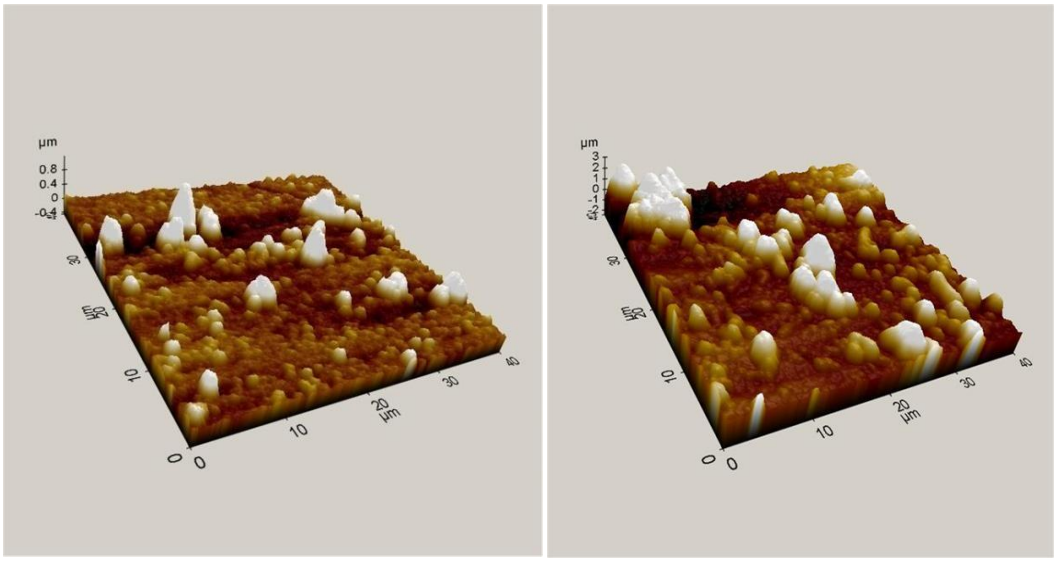

a) b)

Figure 29: Measurement of peak-to-valley roughness index(Ra) of the AFM image PPy-Control sample with vertical height of the image surface of 0.8µm a) and PPy-CNT 0.5 sample with vertical height of the image surface of 3µm b).

4.1.5.2 Profilometer imaging

The coated electrodes surface were further analysed by the Wyko NT1100 optical profilometer. Profilometer images are shown in Figure 25 below. The surface roughness parameter (Rz) was calculated from the Vision64 software. We calculated Rz at two different magnifications of 20x and at 50x. The calculated values is given in Table 5 below.

Table 5: Calculated Surface roughness parameter (Rz) values at 20x and 50x magnifications (µm).

Pt samples	PPy-Control	PPy-CNT 0.1	PPy-CNT 0.25	PPy-CNT 0.5
At 20x (µm)	198	239.2	243.4	228.4
At 50x (µm)	234.8	235.7	245.7	240.2

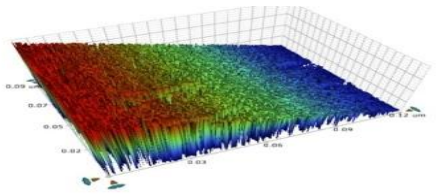

a) PPy-Control (20x)

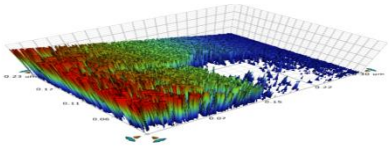

b) PPy-Control (50x)

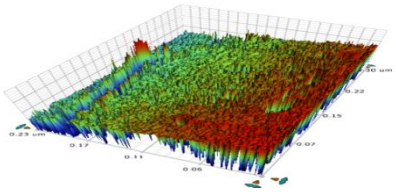

c) PPy-CNT 0.1 (20x)

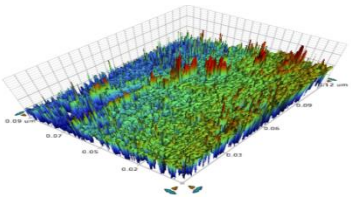

d) PPy-CNT 0.1(50x)

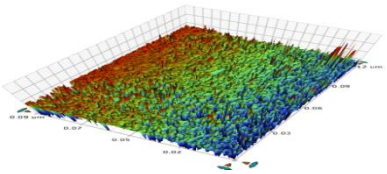

e) PPy-CNT 0.25 (20x)

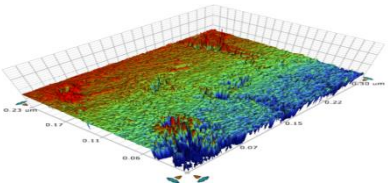

f) PPy-CNT 0.25 (50x)

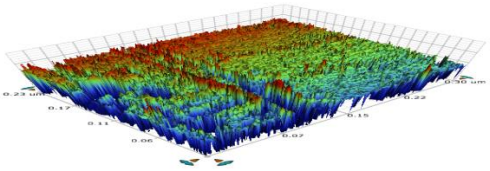

g) PPy-CNT 0.5 (20x)

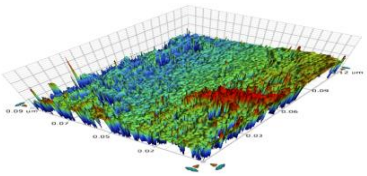

h) PPy-CNT 0.5 (50x)

Figure 30: Profilometer images of PPy-Control (20x) a), PPy-Control (50x) b), PPy-CNT 0.1 (20x) c), PPy-CNT 0.1 (50x) d), PPy-CNT 0.25 (20x) e), PPy-CNT 0.25 (50x) f), PPy-CNT 0.5 (20x) g) and PPy-CNT 0.5 (50x) h). The coating looks pretty dense on the PPy-CNT 0.5 and PPy-CNT 0.25 samples than PPy-Control and PPy-CNT 0.1 samples.

The highest value of Rz was observed in PPy-CNT 0.25 surface which indicates that PPy-CNT 0.25 electrode had the roughest surface compared to other electrodeposition coating. The lowest roughness was observed in PPy-Control film. The order of

roughness in 20x scan was: PPy-CNT 0.25>PPy-CNT0.1>PPy-CNT0.5>PPy-Control while 50x follows: PPy-CNT0.25>PPy-CNT0.5>PPy-CNT0.1>PPy-Control.

4.1.5.3 Micrograph Imaging

The coated samples were imaged with Optical microscope (Olympus BH-2, Olympus Optical Co., Tokyo, Japan) as shown in Figure 26 below. The electrode surface were clearly visible in case of PPy-Control and PPy-CNT 0.1 which indicates that these films were lightly coated. However, electrode surface were almost smoothly coated in case of PPy-CNT 0.25 and PPy-CNT 0.5. Also a thick coating was observed with PPy-CNT 0.25 and PPy-CNT 0.5 micrographs than PPy-Control and PPy-CNT 0.1.

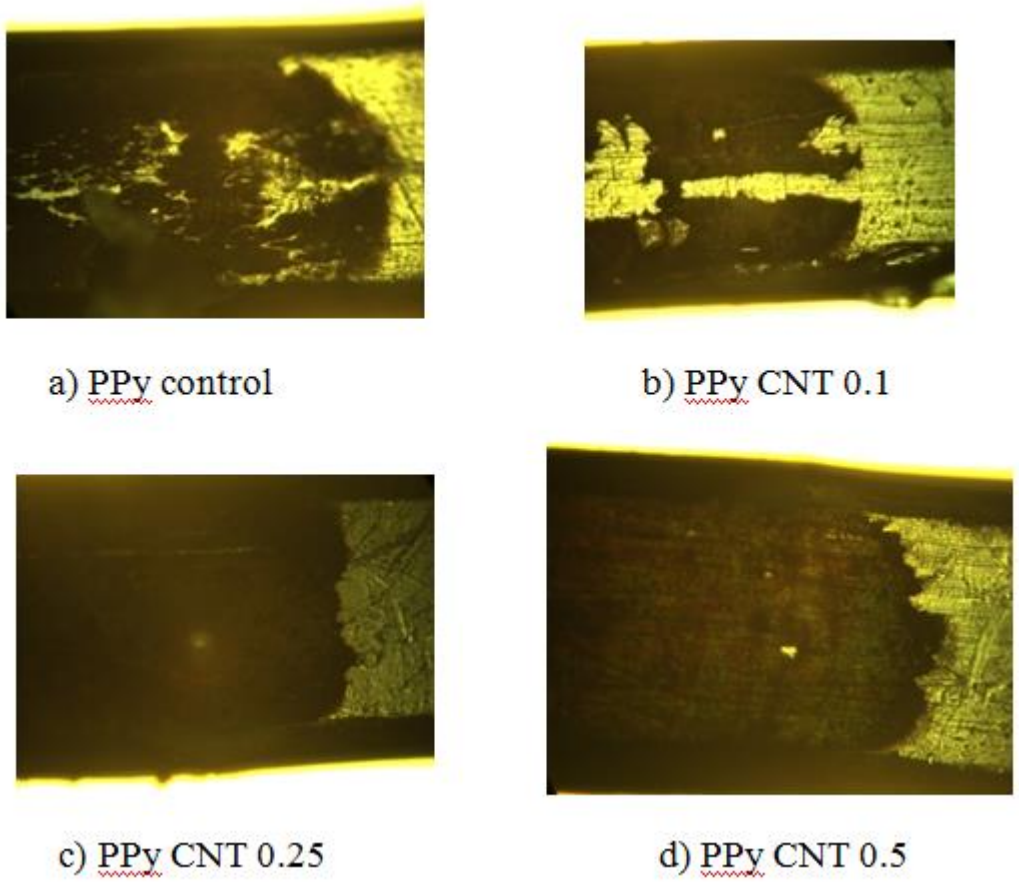

Figure 31: Micrograph images of various PPy/CNT coated samples PPy-Control a), PPy-CNT 0.25 b), PPy-CNT 0.5 c) and PPy-CNT 0.5 d). A darker coating can be seen in case of PPy-CNT 0.25 and PPy-CNT 0.5 than PPy-Control and PPy-CNT 0.1.

4.2 MEA

The polypyrrole-bentzenesulphonate (PPy/DBS) coatings were electrodeposited on platinum microelectrodes. The electrodeposition results are presented in section 4.2.1. The plasma treatment results are presented in section 4.2.2 and the micrograph imaging results are presented in section 4.2.3.

4.2.1 Electrodeposition

Linear Scan Voltammetry technique was used to ramp the voltage from an intial potential to the final potential with the given scan rate. The final potential was then fixed with certain charge limits to generate the current waveform by chronopotentiometry technique. The area of one electrode in MEA was $0.707*10^{-5}cm^2$. This value was fitted to get the desired density curves. Also some of the curves are not drawn to the "end" because the electrodeposition process was stopped because of unstable negative current. The settings is given in Table 6 below.

Table 6: Settings for electrodeposition of PPy/DBS coatings

Electrodes	E17	E54	E47	E52	E62	E73	E65
Initial potential (V)	0	0	0	0	0	0	0
Final potential (V)	1.0	1.0	1.5	1.0	1.3	1.5	1.5
Scan rate (V/s)	0.2	0.2	0.5	0.2	0.2	0.5	0.5
Charge limit (C/cm^2)	7.07	7.07	7.07	7.07	7.07	7.07	7.07

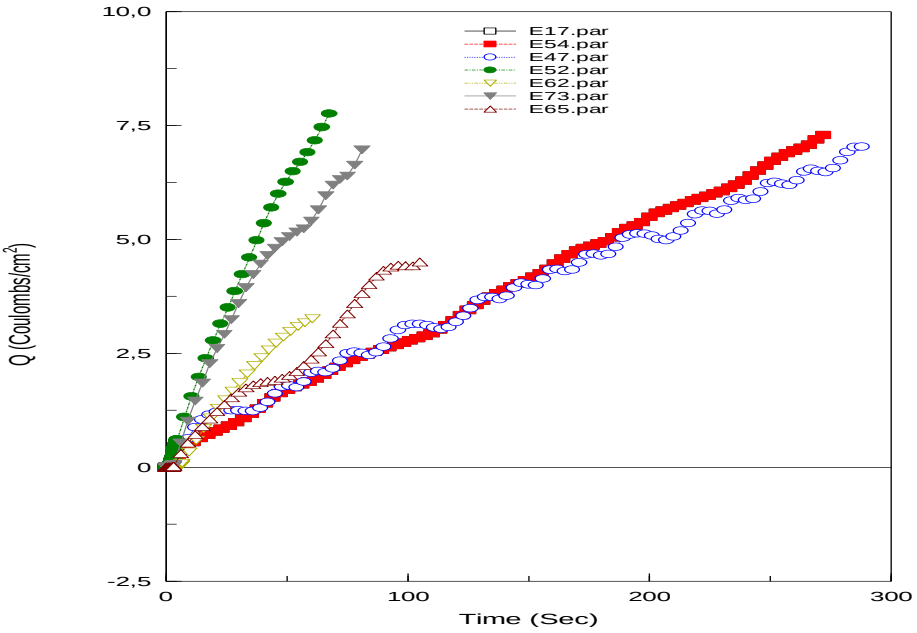

a)

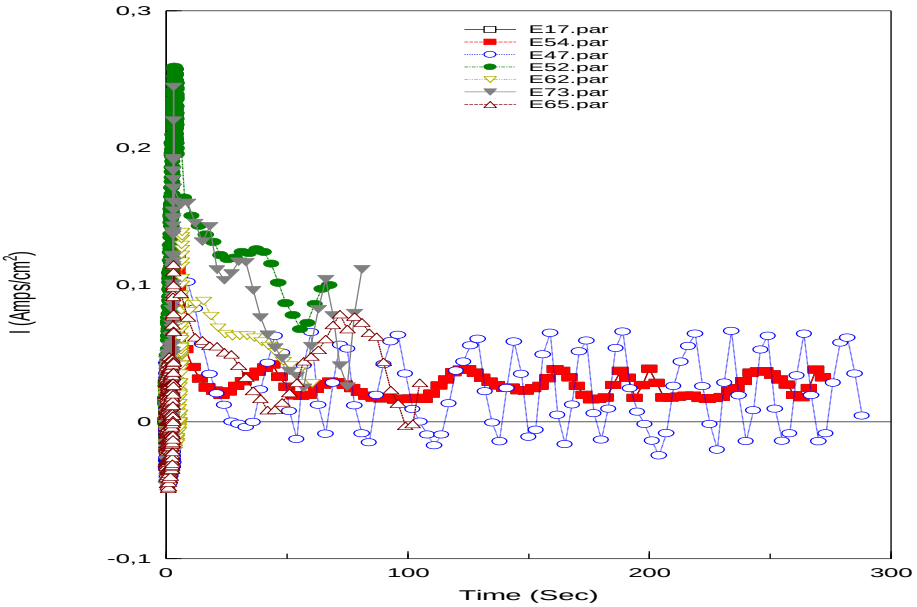

b)

Figure 32: Charge a) and current b) densities during electrodeposition.

We varied the final potential and scan rate of the electrodeposition to test their effect on the electrodeposition process. It was clear from charge density curve that E54 and E47 seemed to be coated for longer duration until 275sec. E62 was found to be coated for shortest of time until70sec. E65 showed similar response as E62. Charge density reached peak with E52 within 70sec which is quickest among any other electrodes. From the current density curve, it was seen that the current was unstable. E54 and E73 showed a large positive current while E17 and E65 showed a negative current within a few milliseconds. Only E54 showed positive current values. No coating of the electrodes were observed which was confirmed by micrograph image and unstable negative current during the polymerization process.

However, variations in the charge and current density was significantly high. E52 had the maximum charge and current density of approximately 7.81C/ cm^2 and 0.26A/ cm^2 respectively while E62 had the minimum charge and current density values of 3.32C/ cm^2 and 0 .14A/ cm^2 respectively. We tried to overcome the problem of unstable negative current during the process by connecting a shunt resistor in the circuit with electrodeposition settings as shown in Table 6 above. However, negative current were still observed with no coating of the electrodes as shown in Figure 27 above.

4.2.1.1 The effect of shunt resistor on electrodeposition process

We used adjustable shunt resistor to overcome the problem of unstable negative current. We used the resistor of 0.5MOhm and 1.0MOhm with charge limits as shown in Table 7 below. The obtained charge and current densities are shown in Fig 28 below.

Table 7: Settings for electrodeposition of PPy/DBS coatings (shunt resistor).

Resistor (MOhm)	0	0	0.5	1.0
Initial potential (V)	0	0	0	0
Final potential (V)	1.0	1.5	1.5	1.5
Scan rate (V/s)	0.5	0.5	0.5	0.5
Charge limit (C/cm^2)	7.07	7.07	7.07	7.07

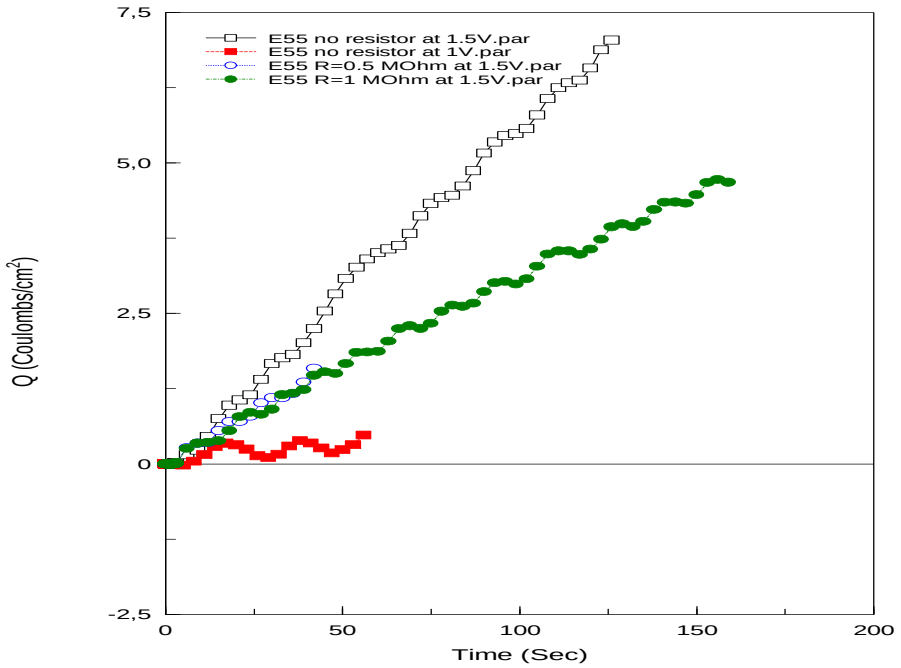

a)

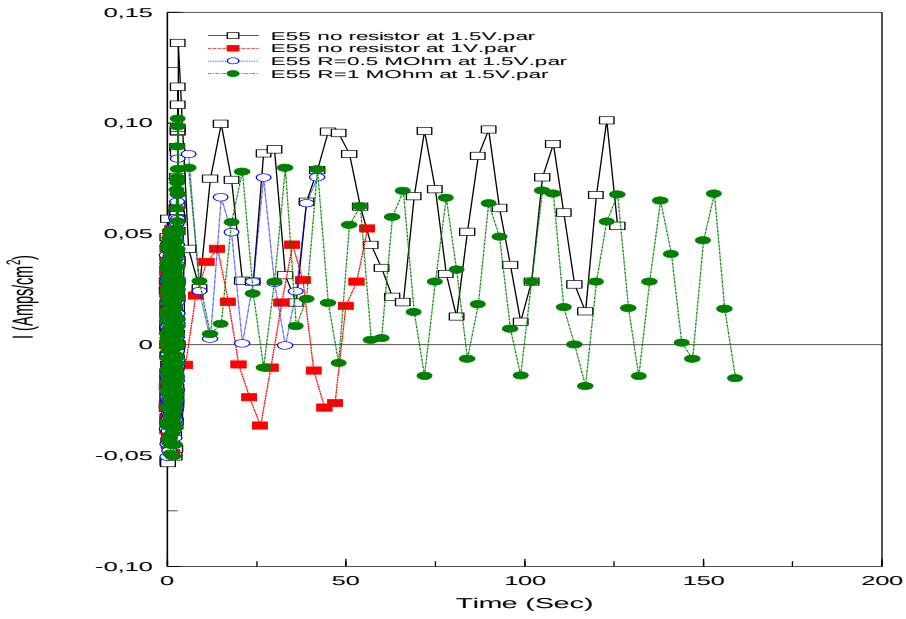

b)

Figure 33: The effect of shunt resistor on electrodeposition process. Charge a) and current b) densities during electrodeposition with and without adjustable shunt resistor.

As seen from charge density curve, the maximum charge density was found with no shunt resistor at 1.5V while with no resistor at 1.0V showed least charge density. Higher resistor value of 1.0MOhm showed higher charge density with longer time duration (160sec) than resistor value of 0.5MOhm, which showed time duration of 40sec. As seen from current density curve, the current values were negative for all electrodeposition. The deposition without resistor at 1.5 V had maximum positive and negative current.

4.2.1.2 The effect of used voltage on electrodeposition process

Since no coating of the electrodes were observed with adjustable shunt resistor, we used further more, different final potentials of 0.9V and 2V along with different charge limits values as shown in above Table 8 to lower the negative current. However, the negative current prevailed in the system with no coating of the electrodes as shown in Figure 29 below.

Table 8: Settings for electrodeposition of PPy/DBS coatings (higher potential).

Electrode	E33	E33
Initial potential (V)	0	0
Final potential (V)	0.9	2
Scan rate (V/s)	0.5	0.5
Charge limit(C/cm^2)	0.14	1.41

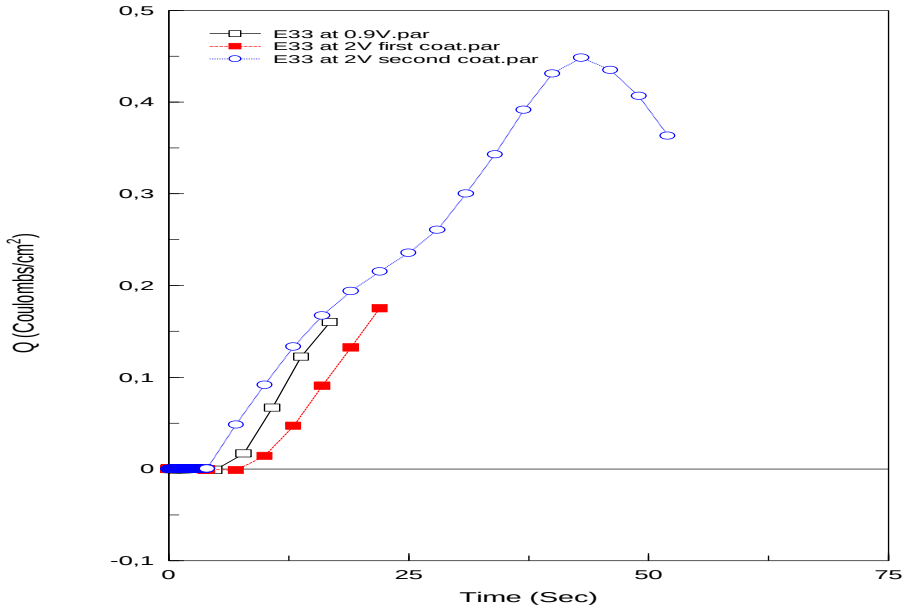

a)

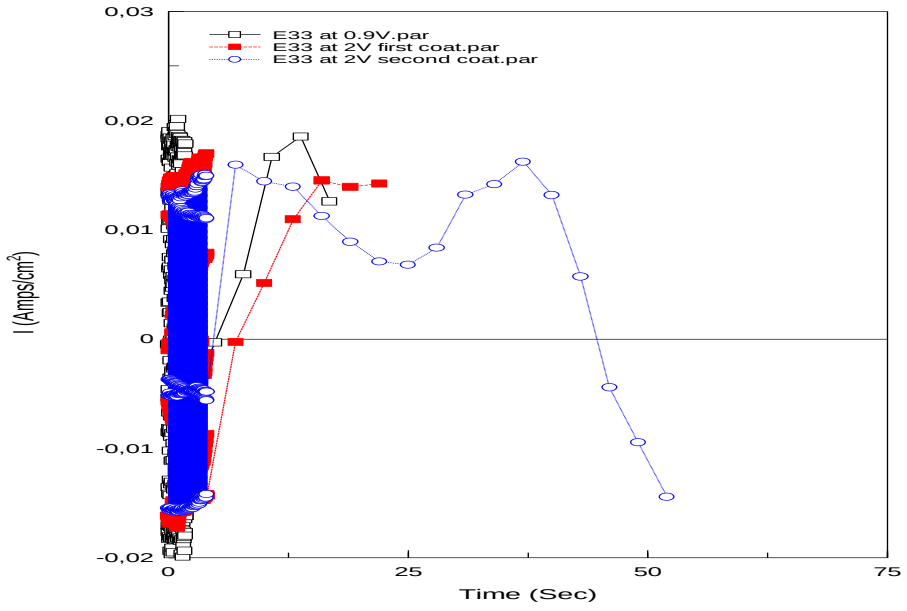

b)

Figure 34: The effect of used voltage on electrodeposision process. Charge a) and current b) densities during electrodeposition of a single microelectrode (E33) at a voltage of 0.9V and 2V.

As seen from charge density curve, electrode coated at lower potential reached maximum charge density while at higher volt couldn't reach at first coat (0.16Q/cm²). However, at the second coat the charge density was risen until 0.45Q/cm² and then decreases. From the current density curve, it was seen that all the electrodeposition showed negative current. The coating at lower potential showed maximum positive and maximum negative values of current density.

4.2.2 Impedance measurements

Pt MEA L1133 was plasma treated and then polymerized. The MEA-IT device was used to measure the impedance at 1.0 kHz of microelectrodes before plasma treatment, after plasma treatment and after polymerization. The measurements of plasma treated plate were done at three time points (30mins, 1h and 2h) after plasma treatment.

4.2.2.1 The effect of plasma treatment on electrode impedance

The impedance of the microelectrode before and after plasma treatment were measured. A significant decrease in impedance magnitude values were observed after plasma treatment. The initial impedance magnitude of the MEA plate was around 80220kOhm before the plasma treatment. The decrease in impedance magnitude was almost four times, around 21800kOhm, when measured after 30 minutes after plasma treatment. Similarly, the impedance was 9530kOhm and 480kOhm after one and two hours of plasma treatment respectively as shown in Figure 30 below. The standard error before plasma treatment was around ±441310kOhm. The standard errors after 30mins, 1h and 2h of plasma treatment were around ±42460kOhm, ±29330kOhmn and ±50kOhm respectively.

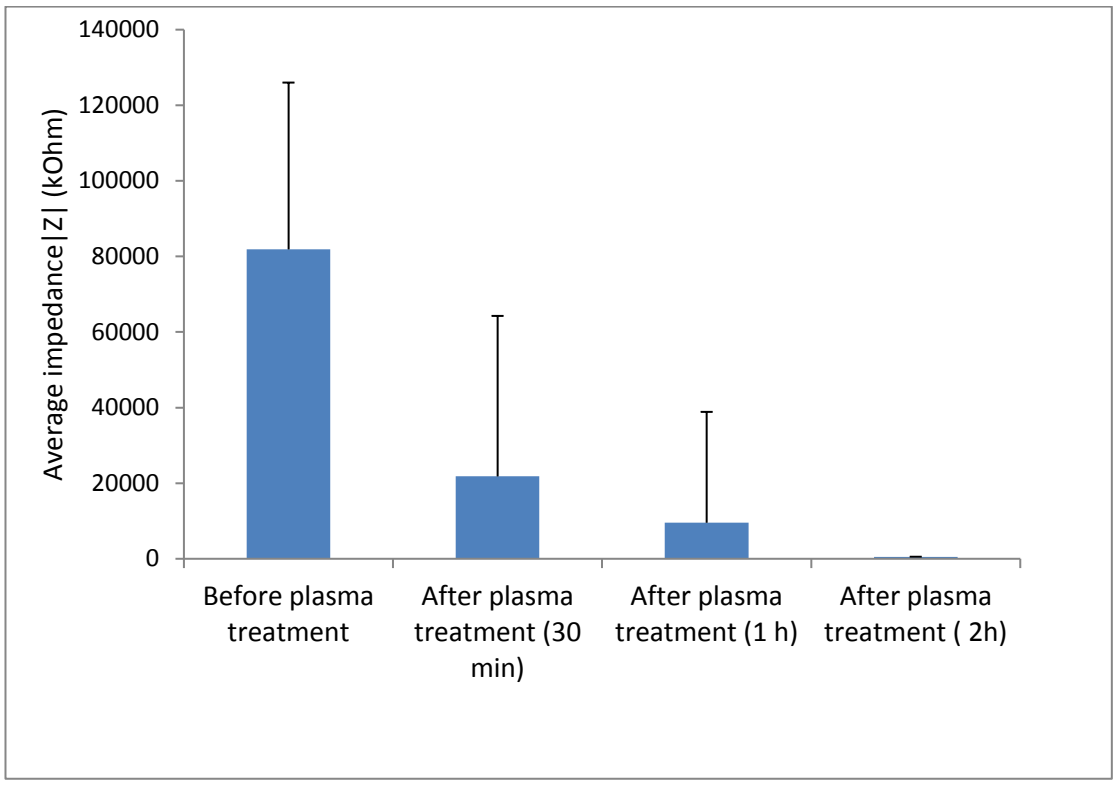

a)

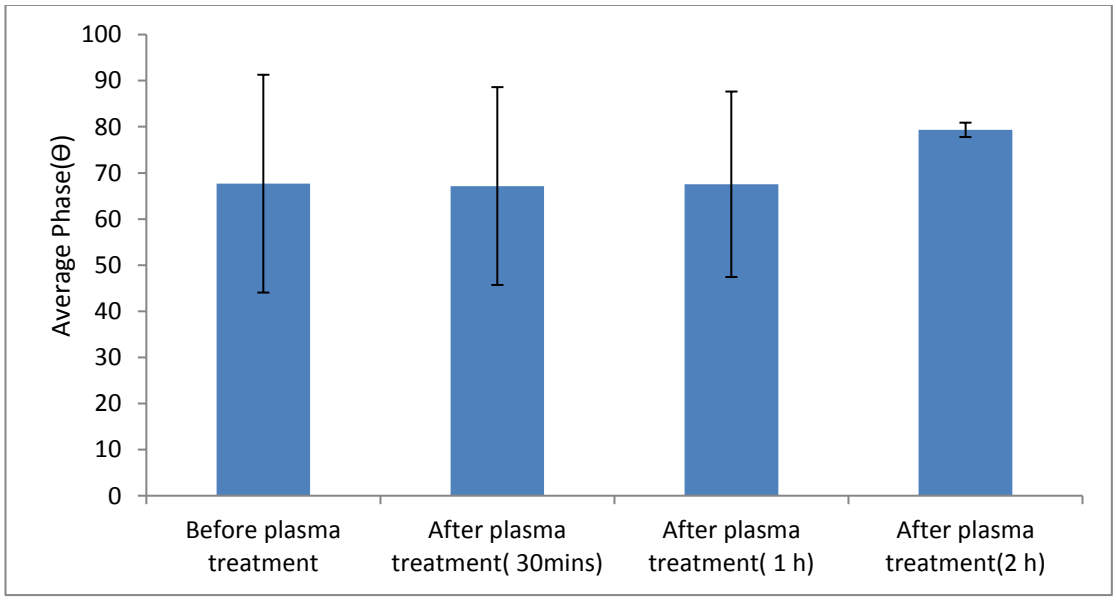

b)

Figure 35: The effect of plasma treatment on the microelectrode plate impedance Impedance magnitude a) and phase b) at the frequency of 1.0 kHz before plasma treatment and after plasma treatment.

The phase angle was almost constant with approximately 67° until the last time point of measurement. However, the phase angle was higher, 80°, when measured after 2h with a large decrease in impedance values shown in Figure. The standard error before plasma treatment was ±23°. The standard errors after 30mins, 1h and 2h of plasma treatment were ±21°, ±20° and ±2° respectively. It was seen that the plasma treatment had completely stabilized the electrode impedance after 2 hours as seen in Figure 31 a) below. The phase angle was maximum after 2 hours of treatment as seen from Figure 31 b). However, not much difference in phase angle was seen after 30mins and 1h of treatment.

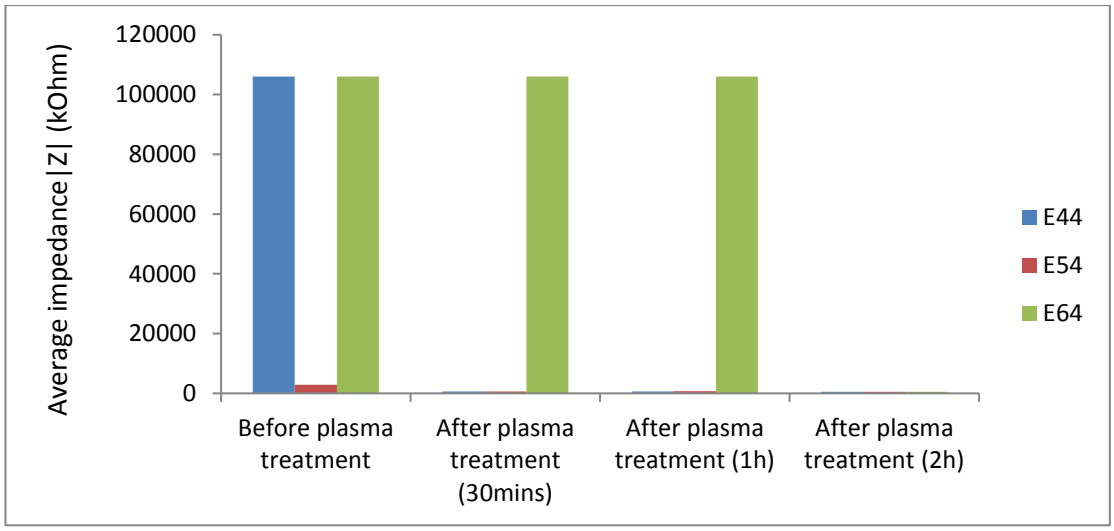

a)

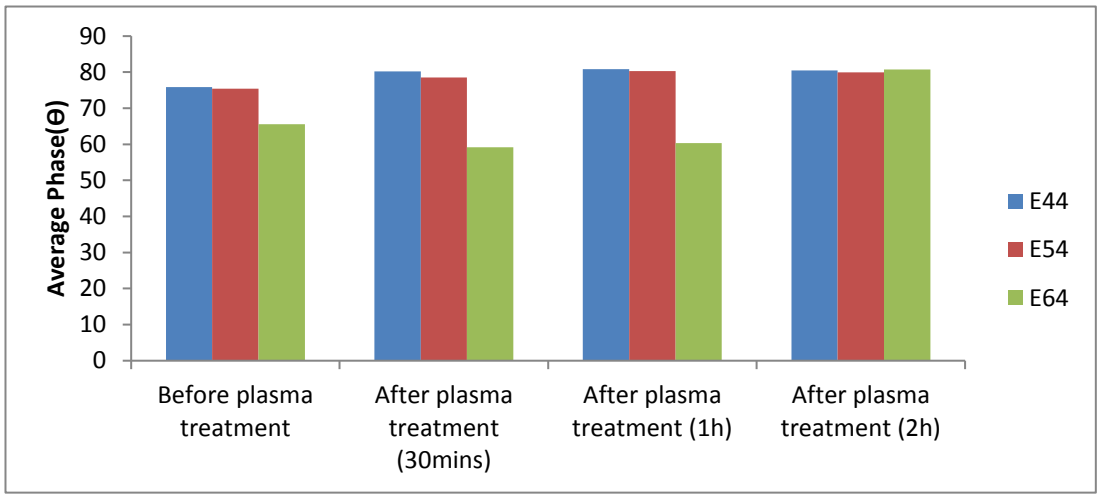

b)

Figure 36: The effect of plasma treatment on the microelectrode impedance: Impedance magnitude a) and phase b) at the frequency of 1.0 kHz before plasma treatment and after plasma treatment.

The impedance of the individual electrodes were measured before and after plasma treatment as shown in Figure 31. The impedance magnitude of E44 before plasma treatment was 106000kOhm. The magnitude was almost half, around530kOhm when measured after 2h of plasma treatment. The magnitude were around 610kOhm and 640kOhm after 30mins and 1h of plasma treatment respectively. The impedance magnitude of E54 before plasma treatment was 2920kOhm. The magnitude was 470kOhm when measured after 2h of plasma treatment. The magnitude after 30mins and 1h of plasma treatment were 670kOhm and 690kOhm respectively. The impedance magnitude of E64 before plasma treatment was 106000kOhm. The magnitude was 510kOhm when measured after 2h of plasma treatment. The magnitude after 30mins and 1h of plasma treatment were both same, 106000kOhm.

The phase angle of E44 before plasma treatment was 75°. The magnitude was 80° when measured after 2h of plasma treatment. The magnitude were 81° and 82° after 30mins and 1h of plasma treatment respectively. The impedance magnitude of E54 before plasma treatment was 75°. The magnitude was 80° when measured after 2h of plasma treatment. The magnitude after 30mins and 1h of plasma treatment were 81° and 80° respectively. The impedance magnitude of E64 before plasma treatment was 65°. The magnitude was 81° when measured after 2h of plasma treatment. The magnitude after 30mins and 1h of plasma treatment were 60° and 61° respectively.

4.2.2.2 The effect of electrodeposition on electrode impedances

The impedance of the individual electrodes E54, E54 and E64 were measured before and after electrodeposition as shown in Figure 32 below. The impedance magnitude of E44 before and after electrodeposition were 106000kOhm and 123kOhm respectively. The impedance magnitude of E54 before and after electrodeposition were 2920kOhm and 620kOhm respectively. The impedance magnitude of E64 before and after electrodeposition were 106000kOhm and 93kOhm respectively.

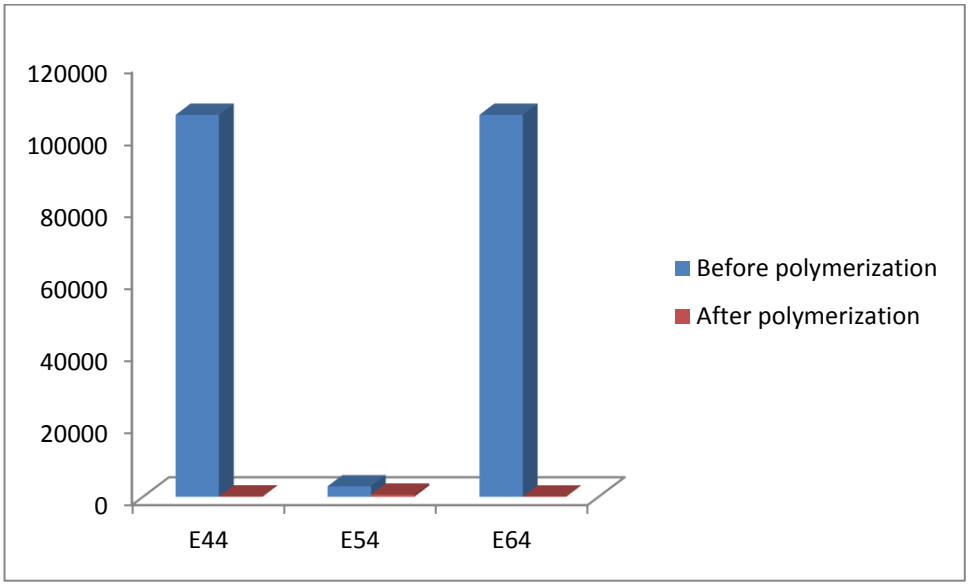

a)

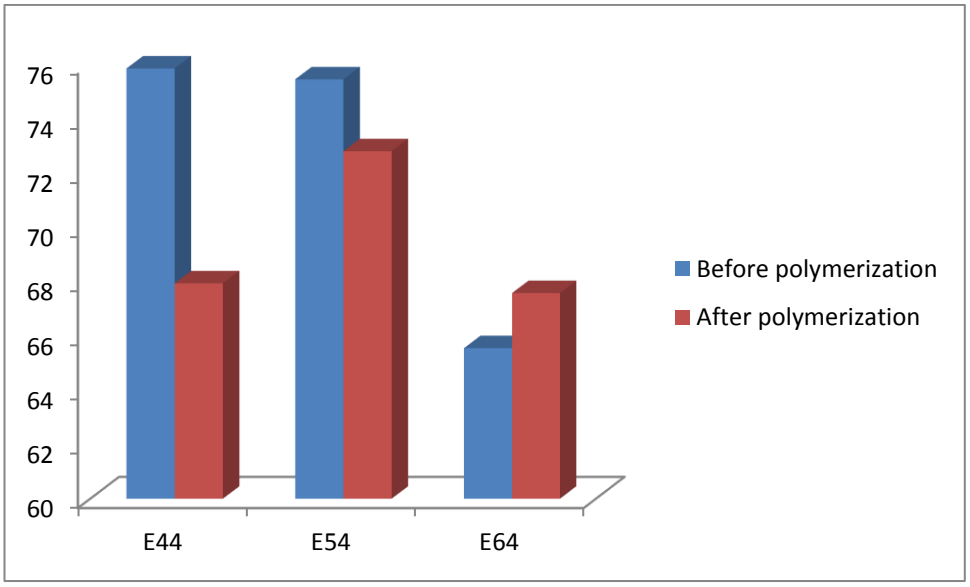

b)

Figure 37: Effect of electrodeposition on the electrode impedance: Impedance magnitude a) and phase b) at the frequency of 1 kHz before polymerization and after polymerization.

The phase angle of E44 before and after electrodeposition were 75° and 67° respectively. The phase angle of E54 before and after electrodeposition were 75° and 72° respectively. Similarly, the phase angle of E64 before and after electrodeposition were 65° and 68° respectively.

4.2.3 Micrograph Imaging

The micrograph images of the MEA plate after electrodeposition of electrodes E44, E54 and E 64 are shown below in Figure 33. It was hard to notice the coating on E44 as seen in Fig 20 b). The electrode "E44" is shown by an arrow. Moreover, the electrolyte solution looked to be spilled between the electrode gaps. It looked as if the plate and electrodes were burned.

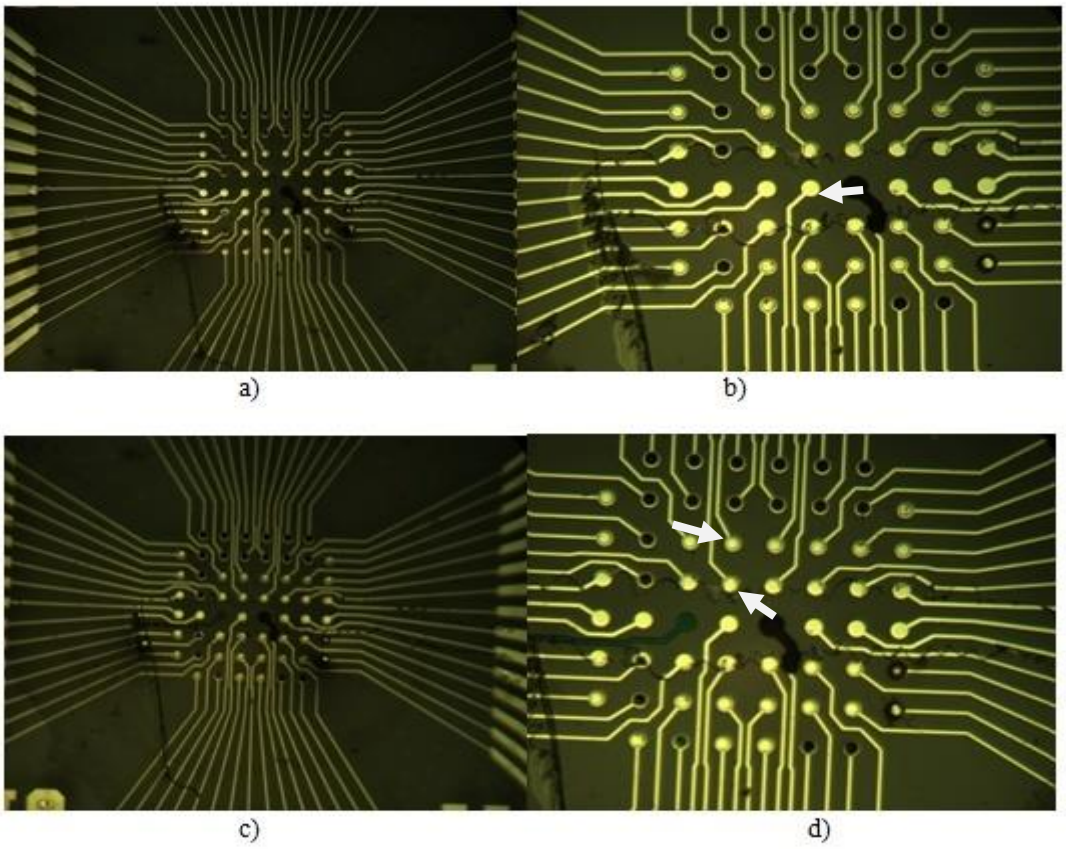

Figure 38: Micrograph imaging of MEA plates E44 (5x) a), E44 (10x) b), E54 and E64 (5x) c) and E54 and E64 (10x) d).

Likewise no coating of the electrodes were observed in E54 and E64 as seen in above Figure 20 d). The electrodes numbers E54 and E64 are shown by an arrow.

5 DISCUSSION AND CONCLUSIONS

The general aim of this project was to coat the electrodes and to measure their electrical properties and also to predict their surface roughness. The aim was also to measure the electrical properties and to predict the roughness of the film by imaging or to observe the effect of coating on the electrode surface.

Firstly, we performed electrochemical deposition of Pt microelectrode using different scan rate of 0.2V/s and 0.5V/s and different final potential of 1.0V, 1.3V and 1.5V. We selected some electrodes for the deposition process and applied different scan time and final potential. No coating of the microelectrodes were observed with PPy solution during the first trial. The polymerization currents were negative and some electrodes even did not reach the maximum charge limit. We tried to overcome this problem by changing the resistance in the circuit by connecting a potentiometer in the electrochemical cell and by plasma treatment. The resistor values used was 0.5MOhm and 1.0MOhm. We changed the scan potential to 0.5V/s and final potential to 1.0V and 1.5V. However, the negative current was still observed. At the third time, we tried to coat the electrodes at higher volts, 2V and also by plasma treatment. But we were not able to get the positive current and we were not able to coat the electrodes.

The plasma treatment was very effective in reducing the electrode impedance however it did not help in coating of the electrodes. The reduction in impedance of plasma treated film were almost only few hundred kOhm compared to impedance of thousands of kOhm of untreated microelectrode plate. The plasma treated plates were also compared with the polymerized plate. A major decrease in impedance magnitude was observed with microelectrodes coating on electrode number 44 (E44) and 54 (E54) at all time points and after electrodeposition process with only few hundred kOhm as shown in Figure 19. The measured phase angle of E44 and E54 looked quite close at each measurement phase with the highest value being close to 80°. The lowest value observed was around 54° with E64. No such measurement for microelectrode has been done before.

We then tried to coat the Pt macroelectrode with PPy and PPy/CNT solutions. We successfully coated the macroelectrode with PPy and PPy/MWCNT composite. Similar coating of PPy-MWCNT composite by electrochemical deposition was also observed in previous research (Shaffer et al. 1998; Han et al. 2005; Almohsin et al. 2012; Li & Zhitomirsky2013). However, in this thesis, results were not very convincing as there was variation and the small concentration of CNT did not improve the electrical properties. However, high concentration of CNT was successful in improving the electrical properties of the coated electrode. The surface properties of PPy changed with the addition of CNT. The PPy/CNT composition produced a more rougher film than the PPy alone. Higher concentration of CNT (PPy-CNT 0.5) film was almost five times more rougher than just PPy film as observed with AFM imaging. The increase in surface roughness with addition of CNT was also observed in previous research

(Almohsin et al. 2012) (Shi & Zhitomirsky 2013). Some previous research showed that the increase in surface roughness of coated electrode contributed to the increase in resistive impedance of the electrode (Xiao et al. 2004) (Cui et al. 2001).

Similarly, the lowest roughness was observed with PPy-Control film as observed with Optical Profilometry. The difference in roughness between PPy and PPy-CNT 0.25 surface was about 45.4µm in 20x scan and 10.9µm. This suggests that the PPy/CNT composite could be useful to produce a rougher electrode surface. This could be of great importance in the future research to predict the electrical behaviour of the electrode-electrolyte interface. This might also help to have a better underestanding of the role of CNT and PPy/CNT in electrochemical deposition. However, some variation in chronopotentiometry measurement in this project was observed which might help to motivate such coating in the future. Overall, this study highlights that the macroelectrode was easily coated than microelectrodes.

6 APPENDIX

Table 9: Pre-treatment of microelectrodes. "-" indicates that no information is given about the subject in the source.

Electrode/Area	Pre-treatment of monomer	pre-treatment of MEAs	References
Au sites(neural probe)/1250µm²	monomer purged with N_2 for 5 mins.	-	(Cuiet al. 2003)
Au/Ir 1250or3900µm²(neural probe)	monomer purged with N_2 for 5 mins.	-	(Cui et al. 2001)
Au/1250 µm² (neural probe)	monomer purged with N_2 for 10 mins.	The probes are degreased in acetic acid (5%), then rinsed several times with water and acetone before electrochemical deposition.	(Yang & Martin 2004)
Au/1250 or 3900µm² (neural probe)/ 16 channel MEAs.	monomer purged with N_2 for 5 mins.	The probes were cleaned for 5 min at 80°C in a base solution containing 1 part ammonium hydroxide, 1 part 30% hydrogen peroxide, and 5 parts deionized water.	(Cui et al. 2001)
36 Au microelectrodes area	degassed by nitrogen stream for PSS and pyrole	-	(Ge et al. 2009)
1.6*10-3cm²/Pt	Pyrole was purified by distillation under reduced pressure	substrate treated with alkysilane.	(Nishizawa et al. 2007)

7 REFERENCES

Abidian, M. R., Kim, D. H., & Martin, D. C. (2006). Conducting polymer nanotubes for controlled drug release. Adv. Mater. (18), 405–409.

Abidian, M. R., Ludwig, K. A., Marzullo, T. C., Martin, D. C., & Kipke, D. R. (2009). Interfacing conducting polymer nanotubes with the central nervous system. Adv.Mater (21), 3764–3770.

Abidian, M. R., & Martin, D. C. (2007). Experimental and theoretical characterization of implantable neural microelectrodes modified with conducting polymer nanotubes. In Biomaterials. Elsevier.

Abidian, M. R., & Martin, D. C. (2009). Multifunctional nanobiomaterials for neural interfaces. Adv. Funct. Mater. (19), 573-585.

Abidian, M. R., Sales, L. G., Yazdan-Shahmorad, A., Marzullo, T. C., & Martin, D. C. (2007). In vivo evaluation of chronically implanted neural microelectrode arrays modified with poly(3,4-ethylenedioxythiophene) nanotubes. . In Proc. 3rd Int. IEEE/EMBS Conf. on Neural Engineering, (pp. 61-64). Kohala Coast: HI.

Agui, L., Yanez-Sedeno, P., & Pingarron, J. M. (2008). Role of carbon nanotubes in electroanalytical chemistry A review. analytica chimica acta, 62, 11–47.

Agui, L., Yanez-Sedeno, P., & Pingarron, J. M. (2008). Role of carbon nanotubes in electroanalytical chemistry A review. analytica chimica acta (622), 11-47.

Almohsin, S. A., AL-Mutoki, S. M., & Li, Z. (2012). Electrochemical Polymerization of PPy-MWCNT composite as a Counter Electrode for Dye-sensitized Solar Cells. Journal of the Arkansas Academy of Science, 66, 31-35.

Ayoub, A., C, S. K., Sahito, I. A., & Jeong, S. H. (2016). Fabrication of textile fabric counter electrode using activated charcoal doped multi walled carbon nanotube hybrid for dye sensitized solar cell. Journal of Materials Chemistry A, 4.

Baranauskas, G., Maggiolini, E., Castagnola, E., Ansaldo, A., Mazzoni, A., Angotzi, G. N., et al. (2011). Carbon nanotube composite coating of neural microelectrodes preferentially improves the multiunit signal-to-noise ratio. Journal of Neural Engineering, 8.

Blau, A., Murr, A., Wolff, S., Sernagor, E., Medini, P., Iurilli, G., et al. (2011). Flexible, all-polymer microelectrode arrays for the capture of cardiac and neuronal signals. Biomaterials, 32, 1778-1786.

Caglar, B. (2017). Production of Carbon Nanotubes by PECVD and Their Applications to Supercapacitors. Barcelona, Spain. Retrieved from http://diposit.ub.edu/dspace/bitstream/2445/11122/1/5NanostructuredMaterials-Caglar-Burak.pdf.

Chemical Derivatization of Microelectrode Arrays by Oxidation of Pyrrole and N-Methylpyrrole: Fabrication of Molecule-Based Electronic Devices1984Journal of American Chemical Society106247389-7396

Chidichimo, G., & Filippelli, L. (2010). Organic Solar Cells: Problems and Perspectives. International Journal of Photoenergy , 1-12.

Cui, X., Hetke, J., Wiler, J., Anderson, D., & Martin, D. (2001). Electrochemical deposition and chaarcaterization of conducting polymer polypyrole/PSS on multichannel neural probes. Sensors and Actuators A, 93 (1), 8-18.

Cui, X., Lee, V. A., Raphael, Y., Wiler, J. A., Hetke, J. F., Anderson, D. J., et al. (2001). Surface modification of neural recording electrodes with conducting polymer/biomolecule blends. J Biomed Mater Res, 56 (2), 261-272.

Cui, X., Wiler, J., Dzaman, M., Altschuler, R. A., & Martin, D. C. (2003). In vivo studies of polypyrrole/peptide coated neural probes. Biomaterials (24), 777-787.

Fei, E., & Brock, R. (2013). Online. https://snsf.stanford.edu/. Retrieved on January 5, 2017, from https://snsf.stanford.edu/equipment/: https://snsf.stanford.edu/equipment/xsa/docs/Park%20XE-100%20User%20Manual.pdf

Foulds, N. C., & Lowe, C. R. (1986). Enzyme entrapment in electrically conducting polymers. J. Chem. Soc. Faraday Trans., I (82), 1259-1264.

Frölich, R., Rzany, A., Riedmüller, J., Bolz, A., & Schaldach, M. (1996). Electroactive coating of stimulating electrodes. J. Mat. Sci. Materials in Medicine, 7, 393-397.

Ge, D., Tian, X., Qi, R., Huang, S., Mu, J., Hong, S., et al. (2009). A polypyrrole-based microchip for controlled drug release. Electrochimica Acta, 55 (1), 271-275.

George, P. M., LaVan, D. A., Burdick, J. A., Chen, C.-Y., Liang, E., & R, L. (2006). Electrically Controlled Drug Delivery from Biotin-Doped Conductive Polypyrrole. Advanced Materials, 18 (5), 577-581.

George, P. M., Lyckman, A. W., LaVan, D. A., Hegde, A., Leung, Y., Avasare, R., et al. (2005). Fabrication and biocompatibility of polypyrrole implants suitable for neural prosthetics. Biomaterials, 26 (17), 3511-3519.

Gerard, M., Chaubey, A., & Malhotra, B. D. (2002). Review. Application of conducting polymers to biosensors. Biosensors & Bioelectronics, 17, 345–359.

Goh, M., Matsushita, S., & Akagi, K. (2009). From helical polyacetylene to helical graphite: synthesis in the chiral nematic liquid crystal field and morphology-retaining carbonisation. Chemical Society Reviews , 2466-2476 .

Han, G., Yuan, G., Shi, G., & Wei, F. (2005). Electrodeposition of polypyrrole/multiwalled carbon nanotube. Thin Solid Films , 64-69.

Harris, A. R., Morgan, S., Chen, J., Kapsa, R. M., & Wallace, G. G. (2013). Conducting polymer coated neural recording electrodes. Journal of Neural Engineering, 10 (1), 1-16.

Harwood, G. W., & Pouton, C. W. (1996). Amperometric enzyme biosensors for the analysis of drug and metabolites. Adv. Drug. Deliv. Rev. , 163-191.

Heim, M., Yvert, B., & Kuhn, A. (2012). Nanostructuration strategies to enhance microelectrode array (MEA) performance for neuronal recording and stimulation. Journal of Physiology, 106 (3-4), 137-145.

Heller, A. (1990). Electrical wiring of redox and enzymes. Acc. Chem. Res., 23, 128-134.

Impedance Testing Device MEA-IT Manual (2013). Online. Reutlingen: Multi Channel Systems MCS GmbH. Retrived on January 5 2017.https://www.multichannelsystems.com/sites/multichannelsystems.com/files/documents/manuals/MEA_Manual.pdf

Indian Instutute of Technology (2010). Online. Retrieved on January 2017, from http://vlab1.iitr.ac.in/: http://vlab1.iitr.ac.in/data/theory/ecg%20theory.pdf

Jacobs, C. B., Peairs, M. J., & Venton, B. J. (2010). Review: Carbon nanotube based electrochemical sensors for biomolecules. Analytica Chimica Acta , 105-127.

Jangid, N. K., Chauhan, N., Ameta, R., & Meghwal, K. (2014). A Review: Conducting Polymers and Their Applications. . Research Journal of Pharmaceutical, Biological and Chemical Sciences , 383-412.

Keefer, E. W., Botterman, B. R., Romero, M. I., Rossi, A. F., & Gross, G. W. (2008, June 29). Carbon nanotube coating improves neural recordings. *Article in Nature Nanotechnology* , pp. 1-6.

Kozai, T. D., Langhals, N. B., Patel, P. R., Deng, X., Zhang, H., Smith, K. L., et al. (2012). Ultrasmall implantable composite microelectrodes with bioactive surfaces for chronic neural interfaces. Nature Materials, 11, 1065-1073.

Kuncel, A. M., & Grill, W. M. (2004). Selection of stimulus parameters for deep brain stimulation. Clinical Neurophysiology, 115 (11), 2431–2441.

LaVan, D. A., George, P. M., & Langer, R. (2003). Simple, three-dimensional microfabrication of electrodeposited structures. Angew Chem, 42 (11), 1262–5.

Li, W., & J, T. (2010). Online.http://ralphgroup.lassp.cornell.edu/index.html. Retrieved on March 19, 2017, from http://ralphgroup.lassp.cornell.edu/index.html: http://ralphgroup.lassp.cornell.edu/projects/graphene_electrochemistry/

Li, X., & Zhitomirsky, I. (2013). Electrodeposition of polypyrroleecarbon nanotube composites for electrochemical supercapacitors. Journal of Power Sources, 221, 49-56.

Li, Y. (2015). Organic Optoelectronic Materials. Suzhou 215123: Springer International Publishing Switzerland 2015.

Lu, Y., Li, T., Zhao, X., Li, M., Cao, Y., Yang, H., et al. (2010). Electrodeposited polypyrrole/carbon nanotubes composite films electrodes for neural interfaces. Biomaterials, 31, 5169-5181.

Marcel, B. (2003). http://www.ece.umd.edu. Retrieved on January 3, 2017, from http://www.ece.umd.edu/MEMS/resources/sop/: http://www.ece.umd.edu/MEMS/resources/sop/VEECO_SOP.pdf

McCreery, D., Agnew, W. F., Yuen, T. G., & Bullara, L. (1990). Charge density and charge per phase as cofactors in neural injury induced by electrical stimulation. EEE Transactions on Biomedical Engineering, 37 (10), 996–1001.

McQuade, D. T., Pullen, A. E., & Swager, T. M. (2000). Conjugated polymer-basedchemicalsensors. Chem. Rev., 100 (7), 2537–2574.

Merkoci, A., Pumera, M., Llopis, X., Perez, B., Valle, M. D., & S, A. (2009). New materials for electrochemical sensing VI: Carbon nanotubes. Trends in Analytical Chemistry , 9.

Merrill, D. R., Bikson, M., & R, J. J. (2005). Electrical stimulation of excitable tissue: design of efficacious and safe protocols. Journal of Neuroscience Methods, 141 (2), 171-198.

Microporous conducting polymers on neural microelectrode arrays I Electrochemical deposition.2004.Sensors and Actuators B1011-2133-142

Neuman, M. R. (2000). The Biomedical Engineering Handbook: Second Edition. Boca Raton: CRC Press LLC.

Nishizawa, M., Nozaki, H., Kaji, H., Kitazume, T., Kobayashi, N., Ishibashi, T., et al. (2007). Electrodeposition of anchored polypyrrole film on microelectrodes and stimulation of cultured cardiac myocytes. Biomaterials, 28 (8), 1480-1485.

Otero, T. F., & Sansinena, J. M. (1998). Soft and wet conducting polymers for artificial muscles. Adv. Mater. (10), 491–494.

Paul, E. W., Ricco, A. J., & Wrighton, M. S. (1985). Resistance of polyaniline films as a function of electrochemical potential and the fabrication of polyaniline-based microelectronic devices. J. Phys.Chem., 89, 1441–1447.

Ravichandran, R., Sundarrajan, S., Venugopal, J. R., Mukherjee, S., & Ramakrishna, S. (2010). Applications of conducting polymers and their issues in biomedical engineering. J. R. Soc. Interface , S559–S579.

Riistama, J. (2010). Characterization of wearable and mplantable Physiological Measurement Devices. Tampere University of Technology .

Sarac, A. S., Ates, M., & Kilic, B. (2008). Electrochemical Impedance Spectroscopic Study of Polyaniline on Platinum, Glassy Carbon and Carbon Fiber Microelectrodes. Int. J. Electrochem. Sci, 3, 777 - 786.

Schmidt, C. E., Shastri, V. R., Vacanti, J. P., & Langer, R. (1997). Stimulation of neurite outgrowth using an electrically conducting polymer. Proc. Natl Acad. Sci. (94), 8948–8953.

Schultze, J. W., & Karabulut, H. (2005). Application potential of conducting polymers. Electrochim. Acta, 50, 1739–1745.

Shaffer, M. S., Fan, X., & Windle, A. H. (1998). Dispersion and Packaging of carbonnanotubesCarbon , 1603-1612.

Shannon, R. V. (1992). A model of safe levels for electrical stimulation. IEEE Trans Biomed Eng, 39 (4), 424-6.

Shi, C., & Zhitomirsky, I. (2013). Electrodeposition of composite polypyrrole–carbon nanotube films. Surface Engineering , 655-661.

Sloten, J. V., Nyssen, V. M., & Haueisen, J. (2008). Coating of neural microelectrodes with intrinsically conducting polymers as a means to improve their electrochemical properties . IFMBE Proceedings 22 (pp. 2409–2412). Berlin: Springer-Verlag.

Stonecypher, L. (2011). Online. http://www.brighthubengineering.com. Retrieved on January 5, 2017, from http://www.brighthubengineering.com/manufacturing-technology/: http://www.brighthubengineering.com/manufacturing-technology/95102-atomic-force-microscopy-afm-contact-non-contact-and-semi-contact-modes/

The Membranes Research Environment (2009). Online.http://membranes.edu.au. Retrieved on January 6, 2017, from http://membranes.edu.au/wiki/index.php/Surface_Roughness: http://membranes.edu.au/wiki/index.php/Surface_Roughness

The Royal Society of Chemistry (2015). Online. http://www.chemspider.com. Retrieved on January 8, 2017, from http://www.chemspider.com/Chemical-

Structure.10606193.html: http://www.chemspider.com/Chemical-Structure.10606193.html

The Royal Swedish Academy of Sciences: The Nobel Prize in Chemistry, 2000: Conductive Polymers, Advanced Information, Stockholm (2000)

Towards real world applications: reproducible and stable PEDOT-CNT microelectrodes.2012.8th Int. Meeting on Substrate-Integrated Microelectrode Arrays, 2012327-328DeizisauIVS Abele GmbH

Unwin, P. R., & Bard, A. J. (1992). Ultramicroelectrode voltammetry in a drop of solution: a new approach to the measurement of adsorption isotherms at solid–liquid interface. Anal. Chem., 64, 113-119.

Vairavapandian, D., Vichchulada, P., & Lay, M. D. (2008). Preparation and modification of carbon nanotubes: Review of recent advances and applications incatalysis and sensing. analytica chimica acta, 626, 119-129.

Vidal, J.-C., Garcia-Ruiz, E., & Castillo, J.-R. (2003). Recent Advances in Electropolymerized Conducting Polymers. Microchim. Acta, 143 (2), 93-111.

Vidu, R., Rahman, M., Mahmoudi, M., Enachescu, M., Poteca, T. D., & Opris, L. (2014). Nanostructures: a platform for brain repair and augmentation. Frontiers in Systems Neuroscience, 8, 1-24.

Volder, M. F., Tawfick, S. H., Baughman, R. H., & Hart, A. J. (2013). Carbon Nanotubes: Present and Future Commercial Applications. Science , 535-539.

Wadhwa, R., Lagenaur, C. F., & Cui, X. T. (2006). Electrochemically controlled release of dexamethasone from conducting polymer polypyrrole coated electrode. Journal of Controlled Release, 110, 531-561.

Weiland, J. D., & Anderson, D. J. (2000). Chronic neural stimulation with thin-film, iridium oxide electrodes. IEEE Trans. Biomed. Eng, 47 (7), 911-918.

Woo, E. J. (2015). Online.http://www.ejwoo.com. Retrieved on March 2017, from http://www.ejwoo.com/biomedical-instrumentation.html: http://iirc.khu.ac.kr/uploads/6/3/4/3/63434825/ch05webster.pdf

Xiao, Y., Cui, X., & Martin, D. C. (2004). Electrochemical polymerization and properties of PEDOT/S-EDOT on neural microelectrode arrays. Journal of Electroanalytical Chemistry, 573, 43-48.

Xiao, Y., Cui, X., Hancock, J. M., Bouguettaya, M., Reynolds, J. R., & Martin, D. C. (2004). Electrochemical polymerization of poly(hydroxymethylated-3,4-ethylenedioxythiophene) (PEDOT-MeOH) on multichannel neural probes. Sensors and Actuators B, 99 (2-3), 437-443.

Xu, L. B., Chen, W., Mulchandani, A., & Yan, Y. (2005). Reversible conversion of conducting polymer films from superhydrophobic to superhydrophilic. . Angew. Chem. Int. , 6009–6012. .

Yang, J., & Martin, D. C. (2004). Microporous conducting polymers on neural microelectrode arrays II. Physical characterization. Sensors and Actuators, 113, 204-211.

Yang, S. Y., Kim, N. H., Cho, Y. S., Lee, H., & Kwon, H. J. (2014). Convallatoxin, a Dual Inducer of Autophagy and Apoptosis, Inhibits Angiogenesis. PLOS ONE, 9.

Zelikin, A. N., D, L., Farhadi, J., Martin, I., Shastri, V., & Langer, R. (2002). Erodible conducting polymers for potential biomedical applications. Angew Chem, 41 (1), 141-4.

Zhong, Y. H., Yu, X. J., Gilbert, R., & Bellamkonda, R. V. (2001). Stabilizing electrode-host interfaces: a tissue engineering approach. . Rehabil. J. Res. Dev. , 627–632.

Ziadan, K. M. (2012). In A. D. Gomes, Conducting Polymers Application, New Polymers for Special Applications. InTech.

Zygo Corporation (2017). Online. https://www.zygo.com. Retrieved March on 5, 2017, from https://www.zygo.com/?/met/profilers: https://www.zygo.com/?/met/profilers/opticalprofilersabout.htm